JHEP

Published for SISSA by Springer

Received: July 15, 2022
Accepted: September 4, 2022
Published: October 13, 2022

Improving methods and predictions at high-energy e^+e^- colliders within collinear factorisation

V. Bertone,[a] **M. Cacciari,**[b,c] **S. Frixione,**[d] **G. Stagnitto,**[e] **M. Zaro**[f] **and X. Zhao**[g]

[a] *IRFU, CEA, Université Paris-Saclay, F-91191 Gif-sur-Yvette, France*
[b] *Sorbonne Université, CNRS, Laboratoire de Physique Thórique et Hautes Énergies, LPTHE, F-75005 Paris, France*
[c] *Université Paris Cité, F-75006 Paris, France*
[d] *INFN, Sezione di Genova, Via Dodecaneso 33, I-16146, Genoa, Italy*
[e] *Physik-Institut, Universität Zürich, Winterthurerstrasse 190, CH-8057 Zürich, Switzerland*
[f] *TIFLab, Università degli Studi di Milano and INFN, Sezione di Milano, Via Celoria 16, I-20133 Milano, Italy*
[g] *Dipartimento di Matematica e Fisica, Università di Roma Tre and INFN, Sezione di Roma Tre, Via della Vasca Navale 84, I-00146 Rome, Italy*

E-mail: valerio.bertone@cern.ch, cacciari@lpthe.jussieu.fr, Stefano.Frixione@cern.ch, giovanni.stagnitto@physik.uzh.ch, Marco.Zaro@mi.infn.it, xiaoran.zhao@uniroma3.it

Abstract: We illustrate how electron Parton Distribution Functions (PDFs) with next-to-leading collinear logarithmic accuracy must be employed in the context of perturbative predictions for high-energy e^+e^--collision processes. In particular, we discuss how the renormalisation group equation evolution of such PDFs is affected by the presence of multiple fermion families and their respective mass thresholds, and by the dependences on the choices of the factorisation and renormalisation schemes. We study the impact of the uncertainties associated with the PDFs on physical cross sections, in order to arrive at realistic precision estimates for observables computed with collinear-factorisation formulae. We do so by presenting results for the production of a heavy neutral object as well as for $t\bar{t}$ and W^+W^- pairs, including next-to-leading-order effects of electroweak origin.

Keywords: Higher Order Electroweak Calculations, Precision QED

ArXiv ePrint: 2207.03265

https://doi.org/10.1007/JHEP10(2022)089

JHEP10(2022)089

Contents

JHEP10(2022)089

1 Introduction

In order to attain the precision goals of future e^+e^- colliders programmes [1–4], computations in perturbative QED play a paramount role, since results obtained at increasingly large orders in the coupling constant α help reduce the theoretical uncertainties that affect them. A key aspect of this kind of predictions is that, on top of being inherently accurate, they give one the ability to assess in a quantitative manner the errors that one makes by identifying them with actual measurements; in fact, such an ability is an integral part of any precision-physics studies.

The calculation of matrix elements of $\mathcal{O}(\alpha^p)$ relative to Born, with $p = 1, 2$ (i.e. next-to-leading order, NLO, and next-to-next-to-leading order, NNLO) and possibly even larger, is a necessary ingredient of accurate results, but not a sufficient one. When integrated over the phase space, such matrix elements give rise to terms of the type $\alpha^p \log^n \mathcal{Q}$, with $\mathcal{Q}$ a small number whose precise nature may depend on the definition of the observable one is looking at, and/or on the characteristics of QED. Depending on $\mathcal{Q}$, one typically has $n \leq p$; thus, the terms above spoil the good behaviour of the perturbative series,[1] and must be resummed. A prominent example of observable-independent logarithmic terms is that for which $\mathcal{Q} = m^2/E^2$, with m the electron mass and E a hard scale typical of the process (e.g. the center-of-mass energy). These terms are present even for fully-inclusive observables, and arise from the collinear emissions off initial- and final-state particles.[2] Here, we shall concentrate on the initial-state case, in view of the fact that the associated logarithms (which we call collinear logarithms, a.k.a. mass singularities in the literature) are ubiquitous, and that those relevant to final-state emissions can be treated in a fully analogous manner. The resummation is carried out in the context of collinear-factorisation formulae [5, 6]; alternative resummation techniques, in particular YFS [7, 8] (that addresses the resummation of soft logarithms) and parton shower [9–12], will not be discussed here.

By writing the collider-level cross section $d\Sigma_{e^+e^-}$ for a generic $e^+e^- \to X$ production process as follows:

$$d\Sigma_{e^+e^-}(P_{e^+}, P_{e^-}) = \sum_{kl} \int dy_+ dy_- \, \mathcal{B}_{kl}(y_+, y_-) \, d\sigma_{kl}(y_+ P_{e^+}, y_- P_{e^-}) \,, \tag{1.1}$$

collinear factorisation amounts to using the following expression:

$$d\sigma_{kl}(p_k, p_l) = \sum_{ij} \int dz_+ dz_- \, \Gamma_{i/k}(z_+, \mu, m) \, \Gamma_{j/l}(z_-, \mu, m) d\hat{\sigma}_{ij}(z_+ p_k, z_- p_l, \mu) \,. \tag{1.2}$$

In eq. (1.1) the functions $\mathcal{B}_{kl}$ account for collective phenomena in beam dynamics, such as beamstrahlung, which give rise to particles k and l, that will eventually initiate the hard scattering. Dominant contributions are those for which the identities of these particles

[1] In fact, the actual behaviour of the series is worse than that, since the coefficient of the $\alpha^p \log^n \mathcal{Q}$ term may also be logarithmically enhanced, by a mechanism different w.r.t. the one that gives rise to $\log \mathcal{Q}$ — the most common example of a double logarithmic enhancement is that due to emissions simultaneously soft and collinear.

[2] Strictly speaking, in the case of bare-lepton observables such logarithms are observable dependent. However, they can be resummed with the same techniques as their observable-independent counterparts.

JHEP10(2022)089

coincide with those of the respective beams (thus, $k = e^+$ and $l = e^-$ here), but others (e.g. $k = \gamma$ and $l = \gamma$) are also interesting; in this paper, we shall limit ourselves to consider only the former. In the collinear-factorisation master formula, eq. (1.2), for any given (k, l) pair the particle-level cross section $d\sigma_{kl}$ is expressed as an incoherent sum of convolutions between parton-level cross sections $d\hat{\sigma}_{ij}$ and PDFs $\Gamma_{\alpha/\beta}(z_\pm)$; each of the latter is the probability density for finding parton α inside particle β with a given fraction $z_\pm$ of the longitudinal momentum of the particle. The PDFs are entirely and solely responsible for resumming the initial-state radiation (ISR) collinear logarithms, and they do so thanks to their being solutions of appropriate renormalisation-group equations [13–16]. As far as the partonic cross sections $d\hat{\sigma}_{ij}$ are concerned, as the notation of eq. (1.2) understands we regard them as computed with massless electrons, all logarithmically dominant mass effects being included in the PDFs; massive-electron results could be employed too (after eliminating double-counting terms), but the differences with the former are only[3] of power-suppressed type, $\mathcal{O}(m^{2q}/E^{2q})$ for some $q \geq 1$. The indices i and j assume values equal to the identities of the partons that emerge from branching processes initiated by the respective particles k and l, compatible with the perturbative order at which the PDFs are computed; in particular, beyond leading order (LO) these include leptons, quarks, and photons, with the dominant contributions being due to $i = k$ and $j = l$.

A common misconception is that eq. (1.2), being based on PDFs obtained by integrating out all non-collinear degrees of freedom, does not give an adequate description of transverse degrees of freedom. We stress that this is certainly not the case, but some clarifications are in order. In the context of a fixed-order computation of $d\hat{\sigma}_{ij}$, the kinematics of the system X and of any recoil partons (i.e. light fermions and photons) that accompany it in the final state is taken into account exactly at the relative order α^p at which the computation is carried out; the higher p, the better the kinematical description (of any degrees of freedom). However, in certain corners of the phase space, e.g. where $p_T(X) \ll E$, this is not relevant, since large logarithmic terms render the order-by-order accurate kinematical description ultimately irrelevant; this is nothing but the emergence of observable-dependent logarithms discussed before (in this example, $\mathcal{Q} = p_T(X)/E$). The solution is to embed the resummation of such logarithms into $d\hat{\sigma}_{ij}$; the crucial point is that this is done *within* a collinear-factorisation approach, not *instead* of it. If this procedure is carried out analytically it usually gives a highly accurate result for the degrees of freedom associated with X, but integrates out those associated with the recoil products. While this is in fact a desirable property in the context of a theory-to-data comparison, it may prevent one from adopting directly at the theoretical level the same cuts as on data, which then must be corrected for that. Again in the context of collinear factorisation, this situation can be further addressed by turning to fully-exclusive predictions, such as those obtained from the aforementioned parton-shower approach or with beyond-LO matching methods that have proven to be extremely effective in hadronic collisions, such as MC@NLO [17] and Powheg [18].

[3]With the exception of Yukawa-induced processes.

JHEP10(2022)089

The bottom line is that, while different strategies exist that one can employ at the short-distance level, they are all underpinned by a collinear *factorisation* picture. Thus, if one is interested in the analysis of the implications of the choice of the PDFs on sufficiently inclusive cross sections, one can essentially adopt the strategy that is most convenient from the computational viewpoint. The obvious candidate is therefore that where cross sections are computed at fixed order; for the purposes of this paper, next-to-leading order accuracy is sufficient, which has the additional benefit of being full automated.

In particular, our goal is that of assessing the impact of the effects due to increasing the accuracy of the PDFs, from LO+leading logarithm (LO+LL) [19–21] to NLO+next-to-leading logarithm (NLO+NLL) [22–24]. We point out that all predictions based on collinear factorisation for e^+e^- cross sections obtained thus far in the literature have employed LO+LL PDFs. In view of the accuracy necessary at future e^+e^- machines this is problematic on at least two counts: it does not match the precision typically available at the matrix-element level and, in keeping with what has been already mentioned at the beginning of this introduction, it does not allow one to properly define a theoretical systematics associated with PDF choices.

While the NLO+NLL results of refs. [22–24] are technically complete, for the goal stated above to be phenomenologically sensible they must be supplemented by a careful treatment of the evolution in the presence of multiple fermion families and their mass thresholds, as well as of the W boson, which was beyond the scope of the original papers. A further interesting aspect is the dependence on the choice of the renormalisation scheme — in refs. [22–24] only $\overline{\text{MS}}$ has been considered. We shall discuss these items in the first part of this paper. Finally, we use this work as an opportunity to upgrade the treatment of e^+e^- ISR effects in the automated framework of MadGraph5_aMC@NLO [25, 26] (called MG5_aMC henceforth) from the LO+LL accuracy [27] to the NLO+NLL one. We stress that this implies that MG5_aMC is now capable of computing NLO EW corrections also for processes with massless initial-state leptons.

This paper is organised as follows. In section 2 we review refs. [22–24] (with additional material reported in appendix D), and discuss the two aspects that must be improved in order to carry out simulations that are phenomenologically viable at high-energy e^+e^- colliders. We deal with them in turn, in section 3 (evolution with multiple fermion families) and section 4 (UV-renormalisation scheme dependence). These sections also present the resulting $z \simeq 1$ analytical forms for the PDFs; the $z < 1$ numerical solutions are discussed in section 5 instead. In section 6 we then use the NLO+NLL PDFs thus obtained to predict observables relevant to the production in e^+e^- collisions of a heavy neutral system, of a W^+W^- pair, and of a $t\bar{t}$ pair. We finally draw our conclusions in section 7. In appendices A and B we give prescriptions relevant to the cases where the perturbative accuracies of the PDFs and the short-distance cross sections are not the same. In appendix C we briefly explain how MG5_aMC has been upgraded for the computations of NLO EW corrections with massless initial-state leptons. Concurrently with this paper, we release a new public version of MG5_aMC, and a code (eMELA) that implements the NLO+NLL PDFs derived here.

JHEP10(2022)089

2 Theoretical ingredients and phenomenological issues

In ref. [22] the NLO-accurate initial conditions for all possible combinations of partons (indices i and j in eq. (1.2)) and particles (indices k and l in eq. (1.2)) have been derived. These are meant to be imposed at a mass scale $\mu_0 \sim m$ and, at variance with their trivial LO counterparts, depend on $\alpha(\mu_0)$ and contain a $\log \mu_0/m$ term. The initial conditions relevant to electrons/positrons (i.e. $k, l = e^{\pm}$) have then been used in refs. [23, 24] to obtain NLL-accurate PDFs, which is all one needs[4] to deal with the largely dominant case where beam dynamics results in particles whose identities are the same as those of the corresponding beams. In the notation of eq. (1.1), this is equivalent to setting:

$$\mathcal{B}_{kl}(y_+, y_-) = \delta_{ke^+}\delta_{le^-}\mathcal{B}_{e^+e^-}(y_+, y_-)\,. \tag{2.1}$$

In view of eq. (2.1), we shall adopt the following simpler notation for the PDFs:

$$\Gamma_{\alpha/e^-} = \Gamma_{\bar{\alpha}/e^+} \equiv \Gamma_\alpha\,, \tag{2.2}$$

where the first equality follows from charge-conjugation invariance, and by $\bar{\alpha}$ we have denoted the antiparticle of α.

While both ref. [23] and ref. [24] work in the $\overline{\text{MS}}$ UV-renormalisation scheme, for the PDFs they adopt different *factorisation* schemes, equal to $\overline{\text{MS}}$ and the so-called Δ, respectively (see ref. [24] for more details). The $\overline{\text{MS}}$- and Δ-defined PDFs have significantly different behaviours at $z \to 1$, in spite of both having an integrable divergence there,[5] whereby this region gives by far the dominant contribution to the cross section independently of the factorisation scheme adopted. The difference due to the factorisation scheme choice in the PDFs is unphysical, and is compensated by its analogue in the partonic cross sections; this compensation can never be exact in physical observables, and thus the residual dependence is typically regarded as a theoretical systematics, which we shall investigate in this paper. Finally, motivated by the dominance of the $z \to 1$ region, one important feature of refs. [23, 24] is the availability of the analytical result for the PDFs in this region: this is crucial in order to obtain numerically-stable integrated predictions.

The results of refs. [23, 24] can immediately be used in eq. (1.2) to predict observables. While from a technical point of view this poses no problem, it is not expected to give a good phenomenological description. The reason is that those PDFs have been derived by considering only the electron, positron, and photon. This is not a issue in itself, and it actually has a clear physical motivation (the effects of other partons being suppressed by at least a relative $\mathcal{O}(\alpha^2)$), but its implication is that, for consistency, α must also be run with a single lepton family; it is known that by doing so one obtains values that lead to a poor description of the data. The solution, which we shall present in section 3, is that of evolving the PDFs by including all of the fermion families in the relevant energy ranges:

[4] We stress that the same methods can be applied to the evolution of other particles, such as photons, should the reason become compelling for also considering these particles as emerging from beam-beam interactions.

[5] More precisely, $\Gamma_{e^\pm/e^\pm}$ has a power-like integrable divergence at $z \to 1$ (accompanied by logarithms in $\overline{\text{MS}}$ but not in Δ), whereas $\Gamma_{\gamma/e^\pm}$ is logarithmically divergent in $\overline{\text{MS}}$; the other PDFs do not diverge.

JHEP10(2022)089

this will allow one to employ a phenomenologically-sound coupling constant, as well as to take automatically into account the $\mathcal{O}(\alpha^2)$ perturbative suppressions mentioned above.

A second item which has not been discussed in refs. [23, 24] is that of the renormalisation-scheme dependence of the PDFs: the results of those papers are relevant to the $\overline{\rm MS}$ scheme. While this is the natural choice in the context of a renormalisation-group evolution (RGE), the existence of phenomenologically appealing renormalisation schemes in the Standard Model alternative to (and much more frequently used than) $\overline{\rm MS}$ motivates the definition of the PDFs in such schemes too. We shall address this point in section 4, both in a general way and by presenting explicit results for the so-called $\alpha(m_Z)$ [28] and G_μ [28, 29] schemes.

We note that while both of the aspects discussed above are relevant to LO+LL PDFs as well, they have been largely ignored in the literature. There are a few reasons for that. Firstly, owing to the LO initial conditions being independent of a small scale (μ_0) and of the coupling constant ($\alpha(\mu_0)$). Secondly, at the LO+LL the running of the coupling constant can formally be neglected. And thirdly, at the LO+LL one simply does not define a theoretical systematics: a choice of parameters is made with a specific application in mind, for which an alternative choice is deemed less suitable, and is thus ignored. In the present work, as far as the choices of settings are concerned, we shall treat the LO+LL and NLO+NLL cases on equal footing, and explore the consequences of this strategy.

3 PDF evolution with multiple fermion families

In order to generalise the results of refs. [23, 24] to the case of several fermions, for a given fermion type f we denote its electric charge (in units of the positron charge) by e_f, its mass by m_f, and its number of colours by $N_c^{(f)}$. The total number of families is denoted by $M = N_l + N_u + N_d$, with N_l leptons, N_u up quarks, and N_d down quarks. With abuse of notation, f can assume both numerical and alpha-numerical values, with the assignments in the former case determined by the hierarchy of the fermion masses:

$$m_1 < m_2 < \ldots < m_M < m_{M+1} \equiv \infty\,. \tag{3.1}$$

Thus, for an electron, $f = e$ or $f = 1$ (and $m_f \equiv m$), the electron being the lightest fermion. The definition of m_{M+1} in eq. (3.1) is a matter of convenience, in that it will simplify some of the formulae to be given below. Our definition for the one-loop charge-renormalisation constant in the $\overline{\rm MS}$ scheme is the following:[6]

$$\begin{aligned} Z_{\alpha_{\overline{\rm MS}}} = \frac{\alpha}{\pi}\Bigg\{ & \frac{1}{3}\sum_{f={\rm light}} N_c^{(f)} e_f^2\,\frac{1}{\bar\epsilon} + \frac{1}{3}\sum_{f={\rm heavy}} N_c^{(f)} e_f^2 \left(\frac{1}{\bar\epsilon} - \log\frac{m_f^2}{\mu^2}\right) \\ & - \frac{7}{4}\left(\frac{1}{\bar\epsilon} - \log\frac{m_W^2}{\mu^2}\right)\Theta(\mu \le m_W) - \frac{7}{4}\,\frac{1}{\bar\epsilon}\,\Theta(\mu > m_W)\Bigg\}, \end{aligned} \tag{3.2}$$

[6] The resulting running coupling constant at scale μ is denoted by $\alpha(\mu)$. It is always clear from the context when one refers to the $\overline{\rm MS}$ coupling, or to the $\alpha(m_Z)$ scheme. Note that in the latter scheme the coupling constant is *not* denoted by $\alpha(m_Z)$, and its value is not equal to $\alpha(m_Z)$ — see section 4.1.

JHEP10(2022)089

where:

$$\frac{1}{\bar{\epsilon}} = \frac{1}{\epsilon} - \gamma_{\rm E} + \log(4\pi)\,. \tag{3.3}$$

For future reference (see section 6) we note that other SM parameters, in particular the masses of the heavy particles, are renormalised on-shell. In the rest of this section, the role of the W will mostly be ignored; we shall discuss it more fully in section 6.1. The "light" and "heavy" fermions (that are summed over in the first and second terms on the r.h.s. of eq. (3.2)) are determined by whether $m_f < \mu$ or $m_f \geq \mu$, respectively, except in the case of the top quark, that is always considered heavy. Equation (3.2) implies that light fermions contribute to the running of α, while heavy fermions decouple. Likewise, the W contributes to the running of α only for scales larger than its mass. More precisely, by defining

$$C^{(a,k)} = \sum_f N_c^{(f)} e_f^a\, \Theta\left(m_f < m_{k+1}\right)\,, \qquad 1 \leq k \leq M\,, \tag{3.4}$$

and by using the conventions of ref. [23] for the coefficients of the β function

$$\frac{\partial\alpha(\mu)}{\partial \log\mu^2} = \beta(\alpha) = b_0\alpha^2 + b_1\alpha^3 + \dots\,, \tag{3.5}$$

in the range

$$m_k \leq \mu < m_{k+1} \tag{3.6}$$

one has $b_0 = b_0^{(k)}$ and $b_1 = b_1^{(k)}$, where:

$$b_0^{(k)} = \frac{C^{(2,k)}}{3\pi} - \frac{7}{4\pi}\,\Theta(\mu > m_W)\,, \qquad b_1^{(k)} = \frac{C^{(4,k)}}{4\pi^2}\,, \tag{3.7}$$

with the coefficient $b_1^{(k)}$ obtained, in pure QED, by imposing at two loops the same decoupling conditions as at one loop. Equation (3.7) formalises the fact that when crossing the mass threshold of fermion k e.g. downwards (i.e. when moving from $\mu = m_k + \varepsilon$ to $\mu = m_k - \varepsilon$) the role of k changes from light to heavy. In keeping with eq. (3.2), $\alpha(\mu)$ is continuous at the thresholds (as well as at the W mass). We shall discuss in section 4 how we determine the value of α at a reference scale, which we shall set equal to the Z mass.

3.1 Structure of the evolution equations

The distinction between light and heavy fermions made above mirrors the usual treatment of these objects in hadronic PDFs, where the latter participate in the evolution only at scales larger than their thresholds; furthermore, PDFs are continuous at such thresholds. It is natural to use the very same approach for electron PDFs. We refrain from repeating here most of the details of the multi-flavour treatment in the context of RGEs, and rather refer the reader to ref. [30], which is particularly convenient because it also presents the explicit results for the Altarelli-Parisi (AP) kernels for any coupling-constant combination $\alpha_S^q\alpha^p$ with $q + p \leq 2$. Clearly, here we are interested in the case $(q, p) = (0, 2)$.

The structure of the evolution equations simplifies considerably if one expresses them in terms of suitable linear combinations of PDFs, as opposed to individual PDFs. There is a certain freedom in their choices; most of the definitions of ref. [30] are well-suited to the

JHEP10(2022)089

computation of the analytical solution in the $z \to 1$ region.[7] In particular, we make use of the non-singlet combinations:

$$\Gamma_{f,\mathrm{NS}} = \Gamma_f - \Gamma_{\bar{f}}\,, \tag{3.8}$$

for any fermion f. The other relevant combinations are the following:[8]

$$\Gamma_{l2} = \Gamma_{e^-} + \Gamma_{e^+} - \left(\Gamma_{\mu^-} + \Gamma_{\mu^+}\right), \tag{3.9}$$

$$\Gamma_{l3} = \Gamma_{e^-} + \Gamma_{e^+} + \Gamma_{\mu^-} + \Gamma_{\mu^+} - 2\left(\Gamma_{\tau^-} + \Gamma_{\tau^+}\right), \tag{3.10}$$

$$\Gamma_{uc} = \Gamma_u + \Gamma_{\bar{u}} - \left(\Gamma_c + \Gamma_{\bar{c}}\right), \tag{3.11}$$

$$\Gamma_{ds} = \Gamma_d + \Gamma_{\bar{d}} - \left(\Gamma_s + \Gamma_{\bar{s}}\right), \tag{3.12}$$

$$\Gamma_{sb} = \Gamma_s + \Gamma_{\bar{s}} - \left(\Gamma_b + \Gamma_{\bar{b}}\right), \tag{3.13}$$

$$\Gamma_{\Sigma^l} = \sum_l^{N_l} \left(\Gamma_{l^-} + \Gamma_{l^+}\right), \tag{3.14}$$

$$\Gamma_{\Sigma^u} = \sum_u^{N_u} \left(\Gamma_u + \Gamma_{\bar{u}}\right), \tag{3.15}$$

$$\Gamma_{\Sigma^d} = \sum_d^{N_d} \left(\Gamma_d + \Gamma_{\bar{d}}\right). \tag{3.16}$$

In addition to these, the photon PDF must be included, whereas the gluon one is ignored.

With the conventions of ref. [23], the perturbative coefficients of the AP kernels relevant to the evolution in the range of eq. (3.6) (i.e. with k light fermions) are defined as follows (in the $\overline{\mathrm{MS}}$ renormalisation scheme):

$$\mathbb{P}^{[k]}(x,\mu) = \sum_{j=0}^{\infty} \left(\frac{\alpha(\mu)}{2\pi}\right)^j \mathbb{P}^{[j,k]}(x)\,, \tag{3.17}$$

where $\mathbb{P}^{[k]}$ and $\mathbb{P}^{[j,k]}$ are matrices whose elements are either the individual AP kernels ($P_{ab}^{[k]}$ and $P_{ab}^{[j,k]}$, if the evolution is carried out in terms of individual PDFs), or some linear combination of them (if the evolution is carried out in terms of singlet and non-singlet combinations of PDFs, as is always the case in practice). Equation (3.17) implies that a given $P_{ab}^{[j,k]}$ in this paper coincides with $P_{ab}^{(0,j+1)}$ of ref. [30] (in that paper, the dependence on the number of light fermions is implicit). In the following, we shall add a lower index N to denote a quantity in Mellin space, which we compute with the standard definition of the Mellin transform:

$$M[f] \equiv f_N = \int_0^1 dz\, z^{N-1} f(z)\,, \qquad \bar{N} = N\, e^{\gamma_{\mathrm{E}}}\,. \tag{3.18}$$

Notation-wise, the upper index $[k]$ on the l.h.s. of eq. (3.17) may be omitted when the corresponding expression is understood to be valid for any k (see e.g. eqs. (3.19)–(3.21)).

[7] Numerically, we solve a marginally different system of equations — see section 5.

[8] These are given for the maximal number of light fermions. When crossing downwards the mass threshold of a given fermion, the corresponding PDF is eliminated from the system, and some PDF combinations become degenerate.

JHEP10(2022)089

In the lepton sector we employ the customary decomposition:

$$P_{l_i l_j} = \delta_{ij} P_{ll}^{\rm V} + P_{ll}^{\rm S}\,, \tag{3.19}$$

$$P_{l_i \bar{l}_j} = \delta_{ij} P_{l\bar{l}}^{\rm V} + P_{l\bar{l}}^{\rm S}\,, \tag{3.20}$$

$$P_{l}^{\pm} = P_{ll}^{\rm V} \pm P_{l\bar{l}}^{\rm V}\,, \tag{3.21}$$

having already used the fact that, up to $\mathcal{O}(\alpha^2)$, $P_{ll}^{\rm S} = P_{l\bar{l}}^{\rm S}$. Equations (3.19)–(3.21) are symbolic both for the full expressions of the kernels, and for each of their perturbative coefficients $P^{[j,k]}$. At the LO there are neither flavour-changing nor singlet contributions, and therefore:

$$P_{l_i l_j,N}^{[0,k]} = \delta_{ij} P_{ll,N}^{{\rm V}[0,k]} \overset{\infty}{=} \delta_{ij} e_l^2 \left(-2\log\bar{N} + \frac{3}{2} - \frac{1}{N}\right)\,, \tag{3.22}$$

$$P_{l_i \bar{l}_j,N}^{[0,k]} = 0\,, \tag{3.23}$$

$$P_{l,N}^{\pm[0,k]} = P_{ll,N}^{{\rm V}[0,k]}\,. \tag{3.24}$$

Here, the symbol $\overset{\infty}{=}$ indicates the fact that, in Mellin space, terms subleading for $N \to \infty$ are neglected. We point out that this operation is only relevant to the analytical computations in the $z \to 1$ region: elsewhere, numerical results that employ the complete expressions of the evolution kernels are used instead. At the NLO, explicit computations that make use of kernels reported in ref. [30] lead to the following expressions:

$$\begin{aligned} P_{ll,N}^{{\rm V}[1,k]} \overset{\infty}{=}\; & e_l^2 \left[\frac{20}{9} C^{(2,k)} \log\bar{N} + e_l^2 \left(\frac{3}{8} - \frac{\pi^2}{2} + 6\zeta_3\right) - \frac{C^{(2,k)}}{18}\left(3 + 4\pi^2\right)\right] \\ & + \frac{e_l^2}{N}\left[-4e_l^2 \log\bar{N} + \frac{27 e_l^2 + 22 C^{(2,k)}}{9}\right]\,, \end{aligned} \tag{3.25}$$

$$P_{l\bar{l},N}^{{\rm V}[1,k]} = \mathcal{O}\left(\frac{1}{N^2}\right)\,, \tag{3.26}$$

$$P_{ll,N}^{{\rm S}[1,k]} = \mathcal{O}\left(\frac{1}{N^3}\right)\,, \tag{3.27}$$

whence:

$$P_{l,N}^{\pm[1,k]} \overset{\infty}{=} P_{ll,N}^{{\rm V}[1,k]}\,. \tag{3.28}$$

From ref. [30] we also obtain the analogous kernels relevant to the quark sector, namely:

$$P_{u,N}^{\pm[j,k]} \overset{\infty}{=} P_{l,N}^{\pm[j,k]}(e_e \to e_u)\,, \tag{3.29}$$

$$P_{d,N}^{\pm[j,k]} \overset{\infty}{=} P_{l,N}^{\pm[j,k]}(e_e \to e_d)\,, \tag{3.30}$$

for both the LO ($j = 0$) and the NLO ($j = 1$) contributions.

A simple algebra leads to the fact that the non-singlet combinations of eq. (3.8) evolve independently, with a kernel equal to P_f^-. Likewise, the PDF combinations of eqs. (3.9)–(3.13) also evolve independently, with a kernel equal to P_l^+ (Γ_{l2} and Γ_{l3}), P_u^+ (Γ_{uc}), and

JHEP10(2022)089

P_d^+ (Γ_{ds} and Γ_{sb}). There thus remain the PDF combinations of eqs. (3.14)–(3.16), plus the photon PDF; these four quantities evolve together, as follows:

$$\frac{d}{d\log\mu^2}\begin{pmatrix}\Gamma_{\Sigma^u}\\ \Gamma_{\Sigma^d}\\ \Gamma_{\Sigma^\ell}\\ \Gamma_\gamma\end{pmatrix} = \begin{pmatrix} P_u^+ + 2N_u P_{uu}^{\rm S} & 2N_u P_{ud}^{\rm S} & 2N_u P_{u\ell}^{\rm S} & 2N_u P_{u\gamma}\\ 2N_d P_{du}^{\rm S} & P_d^+ + 2N_d P_{dd}^{\rm S} & 2N_d P_{d\ell}^{\rm S} & 2N_d P_{d\gamma}\\ 2N_l P_{\ell u}^{\rm S} & 2N_l P_{\ell d}^{\rm S} & P_l^+ + 2N_l P_{\ell\ell}^{\rm S} & 2N_l P_{\ell\gamma}\\ P_{\gamma u} & P_{\gamma d} & P_{\gamma\ell} & P_{\gamma\gamma}\end{pmatrix} \otimes \begin{pmatrix}\Gamma_{\Sigma^u}\\ \Gamma_{\Sigma^d}\\ \Gamma_{\Sigma^\ell}\\ \Gamma_\gamma\end{pmatrix}. \tag{3.31}$$

Equation (3.31) simplifies considerably in the $z \simeq 1$ region, owing to the $N \to \infty$ behaviour of the relevant kernels (see eq. (3.27) — analogous ones holds for quarks). By taking that into account, one arrives at:

$$\frac{d}{d\log\mu^2}\begin{pmatrix}\Gamma_{\Sigma^u,N}\\ \Gamma_{\Sigma^d,N}\\ \Gamma_{\Sigma^l,N}\\ \Gamma_{\gamma,N}\end{pmatrix} \cong \begin{pmatrix} P_{u,N}^+ & 0 & 0 & 2N_u P_{u\gamma,N}\\ 0 & P_{d,N}^+ & 0 & 2N_d P_{d\gamma,N}\\ 0 & 0 & P_{l,N}^+ & 2N_l P_{l\gamma,N}\\ P_{\gamma u,N} & P_{\gamma d,N} & P_{\gamma l,N} & P_{\gamma\gamma,N}\end{pmatrix} \begin{pmatrix}\Gamma_{\Sigma^u,N}\\ \Gamma_{\Sigma^d,N}\\ \Gamma_{\Sigma^l,N}\\ \Gamma_{\gamma,N}\end{pmatrix}. \tag{3.32}$$

At the LO:

$$P_{l\gamma,N}^{[0,k]} \underset{N}{\cong} \frac{e_l^2}{N}, \tag{3.33}$$

$$P_{\gamma l,N}^{[0,k]} \underset{N}{\cong} \frac{e_l^2}{N}, \tag{3.34}$$

$$P_{\gamma\gamma,N}^{[0,k]} \underset{N}{\cong} -\frac{2}{3}C^{(2,k)}, \tag{3.35}$$

while at the NLO:

$$P_{l\gamma,N}^{[1,k]} \underset{N}{\cong} \frac{e_l^4}{N}\left[\log^2\bar{N} + \frac{15-\pi^2}{6}\right], \tag{3.36}$$

$$P_{\gamma l,N}^{[1,k]} \underset{N}{\cong} \frac{e_l^2}{N}\left[-e_l^2\log^2\bar{N} + \frac{15e_l^2 + 4C^{(2,k)}}{3}\log\bar{N} - \frac{3e_l^2(36+\pi^2) + 64C^{(2,k)}}{18}\right], \tag{3.37}$$

$$P_{\gamma\gamma,N}^{[1,k]} \underset{N}{\cong} -C^{(4,k)}. \tag{3.38}$$

The remaining kernels are computed by observing that, at any order:

$$P_{u\gamma} = P_{l\gamma}\left(e_l^a \to N_c e_u^a\right), \qquad P_{d\gamma} = P_{l\gamma}\left(e_l^a \to N_c e_d^a\right), \tag{3.39}$$

$$P_{\gamma u} = P_{\gamma l}\left(e_l \to e_u\right), \qquad P_{\gamma d} = P_{\gamma l}\left(e_l \to e_d\right). \tag{3.40}$$

Equations (3.32)–(3.40) show that, at $\mathcal{O}(N^{-1})$, the singlets couple to each other only through the photon. One is therefore in the same situation as in the single-fermion-family evolution described in detail in appendix B of ref. [23]; we shall exploit this fact in section 3.3.

3.2 Solution of the evolution equations

In this section, we work with the $\overline{\rm MS}$ renormalisation scheme; this condition will be relaxed later (see section 4). However, our treatment applies to any factorisation scheme, although explicit results will be given only for $\overline{\rm MS}$ and Δ.

JHEP10(2022)089

We remind the reader that QED PDFs have a meaningful perturbative expansion at any scale, for whose coefficients we use the same conventions as in eq. (3.17), namely:

$$\Gamma_i(x,\mu) = \sum_{j=0}^{\infty} \left(\frac{\alpha(\mu)}{2\pi}\right)^j \Gamma_i^{[j]}(x,\mu)\,. \tag{3.41}$$

By computing the terms on the r.h.s. of eq. (3.41) from first principles, and by setting $\mu = \mu_0$, with μ_0 a scale of the order of the electron mass, one obtains the initial conditions for the RGE evolution of the PDFs. Up to the NLO [22]:

$$\Gamma_i^{[0]}(z,\mu_0) = \delta_{ie^-}\delta(1-z)\,, \tag{3.42}$$

$$\Gamma_{e^-}^{[1]}(z,\mu_0) = e_e^2\left[\frac{1+z^2}{1-z}\left(\log\frac{\mu_0^2}{m^2} - 2\log(1-z) - 1\right)\right]_+ + e_e^2 K_{ee}(z)\,, \tag{3.43}$$

$$\Gamma_{\gamma}^{[1]}(z,\mu_0) = e_e^2\frac{1+(1-z)^2}{z}\left(\log\frac{\mu_0^2}{m^2} - 2\log z - 1\right) + e_e^2 K_{\gamma e}(z)\,, \tag{3.44}$$

$$\Gamma_i^{[1]}(z,\mu_0) = 0\,, \qquad i \notin \{e^-,\gamma\}\,. \tag{3.45}$$

We point out that while the computation of ref. [22] has been carried out for a single fermion family, its results apply here as well, since at $\mathcal{O}(\alpha)$ the only possible elementary branching is $e \to e\gamma$, whence eq. (3.45) follows trivially. The functions K_{ij} that appear on the r.h.s. of eqs. (3.43) and (3.44) are responsible for defining the factorisation scheme. Technically, they are the finite parts of the subtraction terms for initial-state collinear singularities, the residues of whose poles in $1/\bar{\epsilon}$ are the Altarelli-Parisi kernels; as such, if one works in the $\overline{\text{MS}}$ factorisation scheme one must set them equal to zero. Apart from having to fulfill certain conditions that stem from momentum and charge conservation, these functions are completely arbitrary. This arbitrariness is compensated by an analogous one in the partonic cross sections $d\hat{\sigma}_{ij}$, so that the l.h.s. of eq. (1.2) is independent (at the perturbative accuracy at which one is working) of the choice of the factorisation scheme. At the NLO, the FKS subtraction formalism [31, 32] includes explicitly the functions K_{ij} in the expressions of $d\hat{\sigma}_{ij}$ (in the context of MG5_aMC, see ref. [33]; see also appendix B).

We finally mention the fact that, in keeping with refs. [23, 24], the evolution equations for the PDFs are more conveniently re-expressed as an evolution equation for an evolution operator in Mellin space, $\mathbb{E}_N^{(K)}$. The upper index (K) here reminds one that the evolution operator is dependent on the choice of the factorisation scheme.

3.3 Analytical solution

In order to deal with the running of the coupling constant in an easier manner, in refs. [23, 24] it was shown that in the evolution equation it is convenient to use the variable

$$t = \frac{1}{2\pi b_0}\log\frac{\alpha(\mu)}{\alpha(\mu_0)}\,, \tag{3.46}$$

rather than the scale μ (the two are in one-to-one correspondence). It is immediately clear that eq. (3.46) cannot be used in the presence of mass thresholds, since the value

JHEP10(2022)089

of b_0 depends on the range where the evolution takes place. However, one can easily generalise eq. (3.46). Specifically, by taking eqs. (3.6) and (3.7) into account, we introduce the quantities:

$$\overline{m}_k = \min\Big(m_{k+1}, \max\left(\mu_0, m_k\right)\Big) = \begin{cases} m_k & \mu_0 < m_k \\ \mu_0 & m_k \le \mu_0 < m_{k+1} \\ m_{k+1} & \mu_0 \ge m_{k+1} \end{cases}, \tag{3.47}$$

and we define the analogues of the variable t of eq. (3.46), namely:

$$t_k = \frac{1}{2\pi b_0^{(k)}} \log \frac{\alpha(\mu)}{\alpha(\overline{m}_k)}\,. \tag{3.48}$$

For any k, the variable t_k is the evolution variable to be used instead of μ in the range:

$$m_k \le \mu < m_{k+1} \bigcap \mu \ge \mu_0\,. \tag{3.49}$$

We also need to define:

$$\bar{t}_k = \frac{1}{2\pi b_0^{(k)}} \log \frac{\alpha(m_{k+1})}{\alpha(\overline{m}_k)}\,, \tag{3.50}$$

so that in terms of t_k the range of eq. (3.49) is:

$$0 \le t_k \le \bar{t}_k\,. \tag{3.51}$$

Note that for any k such that $m_{k+1} \le \mu_0$ eq. (3.50) implies that $\bar{t}_k = 0$, and therefore that the range of eq. (3.51) is a zero-measure set where $t_k = 0$. Indeed, in such a case the intersection in eq. (3.49) is the empty set, in keeping with the fact that for scales smaller than μ_0 it is not useful to consider the evolution of the PDFs. In practice, for electron PDFs with $\mu_0 = m$ the range in eq. (3.49) coincides with that in eq. (3.6), and $\bar{t}_k \neq 0$ for any k. Still, eq. (3.51) is fully general, and can be used when $\mu_0 > m$, as well as for PDFs relevant to particles different from the electron, in particular for muons.

In each of the ranges given in eq. (3.51) the evolution operator obeys the same evolution equation as that derived in ref. [24],[9] with the only formal differences due to the coefficients of the β function and to the AP kernels, that here depend on the number of active fermion families. Thus, from eq. (2.25) of ref. [24]:

$$\begin{aligned} \frac{\partial \mathbb{E}_N^{(K)}(t_k)}{\partial t_k} &= b_0^{(k)} \alpha(\mu) \mathbb{K}_N \left(I + \frac{\alpha(\mu)}{2\pi}\,\mathbb{K}_N\right)^{-1} \mathbb{E}_N^{(K)}(t_k) \\ &+ \frac{b_0^{(k)} \alpha^2(\mu)}{\beta(\alpha(\mu))} \sum_{j=0}^{\infty} \left(\frac{\alpha(\mu)}{2\pi}\right)^j \left(I + \frac{\alpha(\mu)}{2\pi}\,\mathbb{K}_N\right) \mathbb{P}_N^{[j,k]} \left(I + \frac{\alpha(\mu)}{2\pi}\,\mathbb{K}_N\right)^{-1} \mathbb{E}_N^{(K)}(t_k)\,. \end{aligned} \tag{3.52}$$

Here, $\mathbb{K}$ is the matrix whose entries are the K_{ij} functions, defined according to the conventions introduced in ref. [24]. As is obvious from eqs. (3.43) and (3.44), here this matrix does not depend on the number of active flavours.

[9] That equation, being valid for a generic factorisation scheme, encompasses and generalises the one introduced in ref. [23], that is relevant to $\overline{\text{MS}}$.

JHEP10(2022)089

As was discussed in section 3.1, the non-singlet combinations of eq. (3.8) evolve independently, with kernels P_f^-. The relevant evolution operator is therefore a scalar, and thus we re-write eq. (3.52) with a simplified notation and by expanding[10] in α:

$$\frac{\partial E_N^{(K)}(t_k)}{\partial t_k} = b_0^{(k)}\alpha(\mu)K_N\left(1+\frac{\alpha(\mu)}{2\pi}K_N\right)^{-1}E_N^{(K)}(t_k) + \left[P_N^{-[0,k]}+\frac{\alpha(\mu)}{2\pi}\left(P_N^{-[1,k]}-\frac{2\pi b_1^{(k)}}{b_0^{(k)}}P_N^{-[0,k]}\right)\right]E_N^{(K)}(t_k)+\mathcal{O}(\alpha^2)\,. \tag{3.53}$$

We point out that, owing to the initial conditions of eqs. (3.42)–(3.45), the only non trivial case for eq. (3.53) is that relevant to the electron non-singlet: we thus understand $P_N^{-[j,k]} \equiv P_{l,N}^{-[j,k]}$ and $K_N \equiv K_{ee,N}$ (incidentally, for all of the other non-singlets the scheme-change kernel is equal to zero). By proceeding as was done in ref. [24], one readily arrives at the solution of eq. (3.53):

$$\log E_N^{(K)}(t_k) = P_N^{-[0,k]}\,t_k + \frac{1}{4\pi^2 b_0^{(k)}}(\alpha(\mu)-\alpha(\overline{m}_k))\left(P_N^{-[1,k]}-\frac{2\pi b_1^{(k)}}{b_0^{(k)}}P_N^{-[0,k]}\right) + \log\frac{1+\frac{\alpha(\mu)}{2\pi}K_N}{1+\frac{\alpha(\overline{m}_k)}{2\pi}K_N}+A_k\,, \tag{3.54}$$

with

$$\alpha(\overline{m}_k) = \alpha(\mu)\,e^{-2\pi b_0^{(k)}t_k}\,, \tag{3.55}$$

and A_k an integration constant, to be determined by imposing suitable initial conditions that we shall soon discuss. We point out that $\overline{m}_k$ is the value of the scale μ when $t_k = 0$, according to eq. (3.48), i.e. of the lower bound on the integration range of eq. (3.49), when the latter is non-trivial.

The determination of the integration constants A_k is done recursively. Firstly, after choosing the scale μ_0 let us denote by ρ an index such that:

$$m_\rho \le \mu_0 < m_{\rho+1}\,. \tag{3.56}$$

Thus, for any $k < \rho$ we have $t_k = 0$ and eq. (3.55) implies that the first three terms on the r.h.s. of eq. (3.54) are equal to zero. Also, below μ_0 there is no evolution, and therefore we must have $E_N^{(K)}(t_k) = I$. Therefore:

$$A_k = 0 \qquad \forall k < \rho\,. \tag{3.57}$$

Exactly the same arguments apply to the case $k = \rho$, since also in this case (owing to the fact that $t_\rho = 0 \Rightarrow \mu = \mu_0$) the initial condition is:

$$E_N^{(K)}(t_\rho = 0) = I\,, \tag{3.58}$$

[10] Note that the inverse operator in the first term on the r.h.s. of eq. (3.52) is not expanded; this is crucial in order to obtain a solution, called Δ_1 in ref. [24], which is sensible at $z \to 1$ — see that paper for more details.

JHEP10(2022)089

and therefore one also has $A_\rho = 0$. Obviously, the fundamental difference between the solutions for $E_N^{(K)}(t_k)$ when $k < \rho$ and $k = \rho$ is that in the former case the entire r.h.s. of eq. (3.54) is equal to zero, while in the latter case only the integration constant (for any $t_\rho > 0$) is equal to zero.

We now consider $k = \rho + 1$. By construction, the lower bound of the integration range in $t_{\rho+1}$, i.e. $t_{\rho+1} = 0$, represents the same scale ($\mu = m_{\rho+1}$) as the upper bound of the integration range in t_ρ, i.e. $t_\rho = \bar{t}_\rho$. At such a scale value, which corresponds to a mass threshold, the PDFs are continuous; in order to achieve this, we impose:

$$\log E_N^{(K)}(t_{\rho+1} = 0) = \log E_N^{(K)}(t_\rho = \bar{t}_\rho)\,. \tag{3.59}$$

By solving eq. (3.59) for $A_{\rho+1}$ we obtain:

$$\begin{aligned} A_{\rho+1} = {} & P_N^{-[0,\rho]}\,\bar{t}_\rho + \frac{\alpha(m_{\rho+1})}{4\pi^2 b_0^{(\rho)}}\left(1 - e^{-2\pi b_0^{(\rho)}\bar{t}_\rho}\right)\left(P_N^{-[1,\rho]} - \frac{2\pi b_1^{(\rho)}}{b_0^{(\rho)}}\,P_N^{-[0,\rho]}\right) \\ & + \log\frac{1 + \frac{\alpha(m_{\rho+1})}{2\pi}K_N}{1 + \frac{\alpha(\overline{m}_\rho)}{2\pi}K_N}\,. \end{aligned} \tag{3.60}$$

which must be replaced in eq. (3.54) in order to obtain the complete solution for $E_N^{(K)}(t_{\rho+1})$. By doing so, it becomes clear how the procedure can be iterated. The result for a generic k (including $k < \rho$) thus reads as follows:

$$\begin{aligned} \log E_N^{(K)}(t_k) = {} & \sum_{i=1}^{k-1} P_N^{-[0,i]}\,\bar{t}_i + P_N^{-[0,k]}\,t_k \\ & + \sum_{i=1}^{k-1}\frac{\alpha(m_{i+1})}{4\pi^2 b_0^{(i)}}\left(1 - e^{-2\pi b_0^{(i)}\bar{t}_i}\right)\left(P_N^{-[1,i]} - \frac{2\pi b_1^{(i)}}{b_0^{(i)}}\,P_N^{-[0,i]}\right) \\ & + \frac{\alpha(\mu)}{4\pi^2 b_0^{(k)}}\left(1 - e^{-2\pi b_0^{(k)}t_k}\right)\left(P_N^{-[1,k]} - \frac{2\pi b_1^{(k)}}{b_0^{(k)}}\,P_N^{-[0,k]}\right) \\ & + \log\left(\frac{1 + \frac{\alpha(\mu)}{2\pi}K_N}{1 + \frac{\alpha(\overline{m}_k)}{2\pi}K_N}\prod_{i=1}^{k-1}\frac{1 + \frac{\alpha(m_{i+1})}{2\pi}K_N}{1 + \frac{\alpha(\overline{m}_i)}{2\pi}K_N}\right)\,. \end{aligned} \tag{3.61}$$

By using the definition of $\overline{m}_i$ given in eq. (3.47), it is immediate to see that:

$$\frac{1 + \frac{\alpha(\mu)}{2\pi}K_N}{1 + \frac{\alpha(\overline{m}_k)}{2\pi}K_N}\prod_{i=1}^{k-1}\frac{1 + \frac{\alpha(m_{i+1})}{2\pi}K_N}{1 + \frac{\alpha(\overline{m}_i)}{2\pi}K_N} = \frac{1 + \frac{\alpha(\mu)}{2\pi}K_N}{1 + \frac{\alpha(\mu_0)}{2\pi}K_N}\,. \tag{3.62}$$

Following refs. [23, 24], in the region of interest ($N \to \infty$) we re-express eq. (3.61) as follows:

$$\log E_N^{(K)}(t_k) \overset{\infty}{=} -\xi_1^{(k)}\log\bar{N} + \hat{\xi}_1^{(k)} + \log\left(\frac{1 + \frac{\alpha(\mu)}{2\pi}K_N}{1 + \frac{\alpha(\mu_0)}{2\pi}K_N}\right)\,, \tag{3.63}$$

JHEP10(2022)089

where we have used eqs. (3.22), (3.24), (3.25), and (3.28) at $\mathcal{O}(N^0)$ to define:

$$\begin{aligned}\xi_1^{(k)}/e_e^2 &= 2\left(\sum_{i=1}^{k-1}\bar{t}_i + t_k\right)\\ &\quad -\sum_{i=1}^{k-1}\frac{\alpha(m_{i+1})}{4\pi^2 b_0^{(i)}}\left(1-e^{-2\pi b_0^{(i)}\bar{t}_i}\right)\left(\frac{20}{9}C^{(2,i)}+\frac{4\pi b_1^{(i)}}{b_0^{(i)}}\right)\\ &\quad -\frac{\alpha(\mu)}{4\pi^2 b_0^{(k)}}\left(1-e^{-2\pi b_0^{(k)}t_k}\right)\left(\frac{20}{9}C^{(2,k)}+\frac{4\pi b_1^{(k)}}{b_0^{(k)}}\right), \qquad (3.64)\\ \hat{\xi}_1^{(k)}/e_e^2 &= \frac{3}{2}\left(\sum_{i=1}^{k-1}\bar{t}_i + t_k\right)\\ &\quad +\sum_{i=1}^{k-1}\frac{\alpha(m_{i+1})}{4\pi^2 b_0^{(i)}}\left(1-e^{-2\pi b_0^{(i)}\bar{t}_i}\right)\left(\lambda_1^{(i)}-\frac{3\pi b_1^{(i)}}{b_0^{(i)}}\right)\\ &\quad +\frac{\alpha(\mu)}{4\pi^2 b_0^{(k)}}\left(1-e^{-2\pi b_0^{(k)}t_k}\right)\left(\lambda_1^{(k)}-\frac{3\pi b_1^{(k)}}{b_0^{(k)}}\right), \qquad (3.65)\end{aligned}$$

with:

$$\lambda_1^{(k)} = e_e^2\left(\frac{3}{8}-\frac{\pi^2}{2}+6\zeta_3\right)-\frac{C^{(2,k)}}{18}\left(3+4\pi^2\right). \qquad (3.66)$$

Noticing that eq. (3.63) has the same functional form as its analogue in the single-fermion-family case of refs. [23, 24], and recalling that the NLO initial conditions are also unchanged, it follows that the $z\to 1$ solution for the electron non-singlet component is obtained from eq. (5.63) of ref. [23] for $\overline{\text{MS}}$, and from eq. (4.40) of ref. [24] for Δ (both are also reported in appendix D), simply with the replacements:

$$\xi_1 \longrightarrow \xi_1^{(k)}, \qquad \hat{\xi}_1 \longrightarrow \hat{\xi}_1^{(k)}. \qquad (3.67)$$

In addition, following the observation about eq. (3.32) that implies that the singlet-photon sector evolution is formally identical to that of refs. [23, 24], we obtain that in the $z\to 1$ region the electron PDF coincide with its non-singlet counterpart, and that the photon PDF can be obtained from eq. (B.87) of ref. [23] for $\overline{\text{MS}}$, and from eq. (5.50) of ref. [24] for Δ (both are also reported in appendix D), again with the replacements of eq. (3.67) and $t\to t_k$.

The results above show explicitly how the PDF evolution with multiple fermion families, although technically more complicated than its single-family counterpart, is qualitatively very similar to the latter, which then provides one with a sensible physical interpretation that is intuitively easier to understand.

4 Alternative UV-renormalisation schemes

In order to obtain the analogues of the results of section 3 in an UV-renormalisation scheme different from $\overline{\text{MS}}$, one starts by observing that the UV-scheme dependence of the PDFs may stem from two different sources: the initial conditions, and the evolution equations.

JHEP10(2022)089

As far as the former are concerned, the NLO initial conditions are in fact UV-scheme independent. This is straightforward to show by using the calculation technique outlined in section 5 of ref. [22], whereby the initial conditions are entirely determined by collinear and quasi-collinear contributions. Therefore, the only possible UV-scheme dependence enters through the coupling constant. Since the first non-null contribution to the initial conditions is of $\mathcal{O}(\alpha^0)$, and since the difference between the coupling constants defined in any two UV schemes is of $\mathcal{O}(\alpha^2)$, if follows that the PDF initial conditions might have a UV-scheme dependence only at the NNLO and beyond.[11]

Coming to the evolution equations, the UV-scheme dependence enters through both the coupling constant and the AP kernels; that of the latter, which starts at the NLO, is in turn also driven by the coupling constant. More specifically, denoting by R a generic non-$\overline{\text{MS}}$ UV-renormalisation scheme,[12] by α_R its coupling constant, and by $\bar{\mathbb{P}}^{[j,k]}$ the matrices of the AP kernels in the R-scheme (i.e. the analogues of the $\overline{\text{MS}}$-defined $\mathbb{P}^{[j,k]}$), we have:

$$\frac{\alpha(\mu)}{2\pi}\sum_{j=0}^{n}\left(\frac{\alpha(\mu)}{2\pi}\right)^j\mathbb{P}^{[j,k]}(x)=\frac{\alpha_R}{2\pi}\sum_{j=0}^{n}\left(\frac{\alpha_R}{2\pi}\right)^j\bar{\mathbb{P}}^{[j,k]}(x,\mu)+\mathcal{O}\left(\alpha^{n+2}\right), \tag{4.1}$$

at any given order α^{n+1}. Here, we shall employ eq. (4.1) at the NLO, i.e. with $n=1$, to obtain $\bar{\mathbb{P}}^{[j,k]}$ in terms of their $\overline{\text{MS}}$ counterparts. In order to do so, we need to express α_R in terms of $\alpha(\mu)$. This is most easily done by expressing α_R in terms of $\alpha(m_Z)$, and then use the RGE of the $\overline{\text{MS}}$ coupling constant to relate $\alpha(m_Z)$ to $\alpha(\mu)$. Note that m_Z is a convenient choice for a "large" scale (i.e. larger than all of the fermion thresholds), given its prominent role in the $\alpha(m_Z)$ and G_μ schemes; if need be, it can be replaced by any other fixed scale. By introducing the coefficient $\Delta_{\overline{\text{MS}}\to R}$ (which is perturbatively calculable) thus:

$$\alpha_R=\alpha(m_Z)-\Delta_{\overline{\text{MS}}\to R}\,\alpha^2(m_Z)+\mathcal{O}(\alpha^3), \tag{4.2}$$

we obtain:

$$\bar{\mathbb{P}}^{[0,k]}(x,\mu)=\mathbb{P}^{[0,k]}(x), \tag{4.3}$$

$$\bar{\mathbb{P}}^{[1,k]}(x,\mu)=\mathbb{P}^{[1,k]}(x)+\left(2\pi b_0^{(k)}\log\frac{\mu^2}{m_{k+1}^2}+D^{(k)}\right)\mathbb{P}^{[0,k]}(x), \tag{4.4}$$

having now defined

$$m_{M+1}=m_Z \tag{4.5}$$

and

$$D^{(k)}=2\pi\sum_{i=k+1}^{M}b_0^{(i)}\log\frac{m_i^2}{m_{i+1}^2}+2\pi\Delta_{\overline{\text{MS}}\to R}. \tag{4.6}$$

[11] Note, however, that it is not mandatory to expand perturbatively the α factor that appears in the NLO contribution to the PDF initial conditions in terms of a given reference coupling; for the sake of numerical accuracy, it is actually better to employ the value dictated by the specific UV scheme chosen. By doing so, the *numerical* values of the PDF initial conditions at the NLO are dependent on the UV scheme, but it remains true that, from a perturbative standpoint, such a dependence is of higher order.

[12] Since in practice we shall employ either the $\alpha(m_Z)$ or the G_μ scheme as alternatives to $\overline{\text{MS}}$, the discussion that follows assumes that the coupling constant defined in R does not run. It is trivial to generalise the results to the cases where this condition is relaxed.

JHEP10(2022)089

In eq. (4.6) we understand that the sum in the first term on the r.h.s. gives no contribution when $k = M$, i.e. $D^{(M)} = 2\pi\Delta_{\overline{\rm MS}\to R}$.

In view of the fact that we are considering here a scheme R where the coupling constant does not run (see footnote 12), the evolution equation for the evolution operator is best expressed directly in terms of the scale μ. Following ref. [24], it is straightforward to arrive at the following result:

$$\frac{\partial \mathbb{E}_N^{(K)}(\mu)}{\partial \log \mu^2} = \sum_{j=0}^{\infty} \left(\frac{\alpha_R}{2\pi}\right)^{j+1} \left(I + \frac{\alpha_R}{2\pi}\,\mathbb{K}_N\right) \bar{\mathbb{P}}_N^{[j,k]} \left(I + \frac{\alpha_R}{2\pi}\,\mathbb{K}_N\right)^{-1} \mathbb{E}_N^{(K)}(\mu)\,, \tag{4.7}$$

which is the counterpart of eq. (3.52), understood to be relevant in the following range:[13]

$$\begin{aligned} &m_k \le \mu < m_{k+1} \bigcap \mu \ge \mu_0\,, \quad && k \le M-1\,, \\ &\mu \ge m_M \bigcap \mu \ge \mu_0\,, && k = M\,. \end{aligned} \tag{4.8}$$

As we have seen in section 3.3, if one is interested in the $z \to 1$ behaviour the only non-trivial content of eq. (4.7) is that relevant to the non-singlet electron component. In that case, by applying the same iterative procedure as in section 3.3, we arrive at the following solution

$$\log E_N^{(K)}(\mu) \overset{\infty}{=} -\xi_1^{(k)} \log \bar{N} + \hat{\xi}_1^{(k)}\,, \tag{4.9}$$

where:

$$\begin{aligned} \xi_1^{(k)}/e_e^2 = {} & \frac{\alpha_R}{\pi}\left(\log\frac{\mu^2}{\overline{m}_k^2} + \sum_{i=1}^{k-1}\log\frac{m_{i+1}^2}{\overline{m}_i^2}\right) \\ & + \frac{\alpha_R^2}{2\pi}\left\{ b_0^{(k)}\left(\log^2\frac{\mu^2}{m_{k+1}^2} - \log^2\frac{\overline{m}_k^2}{m_{k+1}^2}\right) - \sum_{i=1}^{k-1} b_0^{(i)}\log^2\frac{\overline{m}_i^2}{m_{i+1}^2} \right. \\ & \quad - \frac{1}{\pi}\left(\frac{10}{9}C^{(2,k)} - D^{(k)}\right)\log\frac{\mu^2}{\overline{m}_k^2} \\ & \quad \left. - \frac{1}{\pi}\sum_{i=1}^{k-1}\left(\frac{10}{9}C^{(2,i)} - D^{(i)}\right)\log\frac{m_{i+1}^2}{\overline{m}_i^2}\right\}, \end{aligned} \tag{4.10}$$

$$\begin{aligned} \hat{\xi}_1^{(k)}/e_e^2 = {} & \frac{3\alpha_R}{4\pi}\left(\log\frac{\mu^2}{\overline{m}_k^2} + \sum_{i=1}^{k-1}\log\frac{m_{i+1}^2}{\overline{m}_i^2}\right) \\ & + \frac{3\alpha_R^2}{8\pi}\left\{ b_0^{(k)}\left(\log^2\frac{\mu^2}{m_{k+1}^2} - \log^2\frac{\overline{m}_k^2}{m_{k+1}^2}\right) - \sum_{i=1}^{k-1} b_0^{(i)}\log^2\frac{\overline{m}_i^2}{m_{i+1}^2}\right\} \\ & + \left(\frac{\alpha_R}{2\pi}\right)^2\left\{ \lambda_1^{(k)}\log\frac{\mu^2}{\overline{m}_k^2} + \sum_{i=1}^{k-1}\lambda_1^{(i)}\log\frac{m_{i+1}^2}{\overline{m}_i^2} \right. \\ & \quad \left. + \frac{3}{2}\left(D^{(k)}\log\frac{\mu^2}{\overline{m}_k^2} + \sum_{i=1}^{k-1} D^{(i)}\log\frac{m_{i+1}^2}{\overline{m}_i^2}\right)\right\}. \end{aligned} \tag{4.11}$$

[13] Equation (4.8) is identical to eq. (3.49); they seemingly differ because of the different definitions of m_{M+1} in eqs. (3.1) and (4.5).

JHEP10(2022)089

Equations (4.10) and (4.11) must be used on the r.h.s.'s of the replacements of eq. (3.67), together with the replacement

$$\alpha(\kappa) \longrightarrow \alpha_R \tag{4.12}$$

for any scale κ, in order to obtain the $z \to 1$ solution for the electron PDF in the R UV-renormalisation scheme from eq. (5.63) of ref. [23] (in the $\overline{\text{MS}}$ factorisation scheme), and from eq. (4.40) of ref. [24] (in the Δ factorisation scheme) — these equations are also reported in appendix D.

By means of a straightforward algebra,[14] one can verify that the expansions in series of α of eqs. (4.10) and (4.11) differ from those of eqs. (3.64) and (3.65), respectively, by terms of $\mathcal{O}(\alpha^3)$. Conversely, these differences are of $\mathcal{O}(\alpha^2)$ if in the $\overline{\text{MS}}$ results of eqs. (3.64) and (3.65) one naively neglects the running of α (by fixing the value of $\alpha(\mu)$ and by setting the β-function coefficients equal to zero in the analytical expressions). Because of this, in order to study the behaviour of the NLL PDFs at fixed α, one must choose a renormalisation scheme where α does not run, as opposed to simply switching the running of α off in $\overline{\text{MS}}$ (as one can do at the LL). Having said that, we note that the $\mathcal{O}(\alpha^3)$ terms mentioned above are logarithmically enhanced (by $\log \mu^2$); therefore, we expect these differences to become more relevant with increasing energies. We shall briefly return to this matter in section 6.3.

4.1 The $\alpha(m_Z)$ and G_μ schemes

In this section we give the relevant definitions for the α renormalisation factors in the $\alpha(m_Z)$ and G_μ schemes, whose associated coupling constants we denote by α_{m_Z} and α_{G_μ}, respectively. We also compute their numerical values, as well as that of the $\overline{\text{MS}}$ coupling at $\mu = m_Z$, i.e. $\alpha(m_Z)$, which we shall eventually use in our numerical simulations of section 6. We work at the one-loop level, and we employ the notation of ref. [29] for the two-point functions.

We start from the so-called $\alpha(0)$ scheme, for which:

$$Z_{\alpha(0)} = \Pi^{AA}(0) - 2\frac{s_W}{c_W}\frac{\Sigma_T^{AZ}(0)}{m_Z^2}\,, \tag{4.13}$$

where

$$s_W = \sqrt{1-c_W^2}\,, \qquad c_W = \frac{m_W}{m_Z}\,, \tag{4.14}$$

and

$$\Pi^{AA}(0) = \left.\frac{\partial\Sigma_T^{AA}(k^2)}{\partial k^2}\right|_{k^2=0}\,, \qquad \Pi^{AA}(k^2) = \frac{\Sigma_T^{AA}(k^2)}{k^2}\,. \tag{4.15}$$

The corresponding coupling constant is equal to the Thomson value:

$$\alpha(0) = 1/137.035999084\,. \tag{4.16}$$

The two-point $\gamma\gamma$ function is conveniently decomposed into its fermion and W contributions:

$$\Pi^{AA}(0) = \sum_f \Pi_f^{AA}(0) + \Pi_W^{AA}(0)\,. \tag{4.17}$$

[14] This entails expanding in series of α the parameters t_k and $\bar{t}_k$, and employing eq. (4.2).

JHEP10(2022)089

The renormalisation constant for α in the $\alpha(m_Z)$ scheme is defined as follows

$$Z_{\alpha(m_Z)} = Z_{\alpha(0)} - \Delta\alpha\,, \tag{4.18}$$

with

$$\Delta\alpha = \sum_{f=\text{light}} \left(\Pi_f^{AA}(0) - \Pi_f^{AA}(m_Z^2)\right) \equiv \Delta\alpha_L^{(3)} + \Delta\alpha_H^{(5)}\,. \tag{4.19}$$

In the rightmost side of eq. (4.19) we have separated the leptons and the light-quark contributions, thus:

$$\Delta\alpha_L^{(3)} = \sum_{\ell} \left(\Pi_\ell^{AA}(0) - \Pi_\ell^{AA}(m_Z^2)\right) \overset{\text{pert}}{=} \sum_{\ell} P_f\left(m_\ell, m_Z\right)\,, \tag{4.20}$$

$$\Delta\alpha_H^{(5)} = \sum_{q=\text{light}} \left(\Pi_q^{AA}(0) - \Pi_q^{AA}(m_Z^2)\right) \overset{\text{pert}}{=} \sum_{q=\text{light}} P_f\left(m_q, m_Z\right)\,, \tag{4.21}$$

with:

$$P_f\left(m, Q\right) = \frac{\alpha}{3\pi} N_c^{(f)} e_f^2 \left(\log\frac{Q^2}{m^2} - \frac{5}{3}\right) + \mathcal{O}\left(\frac{m^2}{Q^2}\right). \tag{4.22}$$

As the notation of eqs. (4.20) and (4.21) suggests, all three leptons and all the quarks except the top are considered to be light, which is in keeping with the fact that we work at the Z mass. The symbol $\overset{\text{pert}}{=}$ indicates that the result on its right is obtained by means of a perturbative computation of the relevant two-point functions; at one loop, this gives eq. (4.22) — the power-suppressed terms on the r.h.s. are known exactly, and are omitted here only for the sake of brevity. From eqs. (4.13), (4.18), (4.20), and (4.21) we obtain:

$$Z_{\alpha(m_Z)} = \sum_{f=\text{heavy}} \Pi_f^{AA}(0) + \sum_{f=\text{light}} \Pi_f^{AA}(m_Z^2) + \Pi_W^{AA}(0) - 2\frac{s_W}{c_W}\frac{\Sigma_T^{AZ}(0)}{m_Z^2}\,. \tag{4.23}$$

With an explicit computation, this leads to the following expression:

$$\begin{aligned} Z_{\alpha(m_Z)} = \frac{\alpha}{\pi}\Bigg\{ & \frac{1}{3}\sum_{f=\text{light}} N_c^{(f)} e_f^2 \left(\frac{1}{\bar{\epsilon}} + \frac{5}{3} - \log\frac{m_Z^2}{\mu^2}\right) \\ & + \frac{1}{3}\sum_{f=\text{heavy}} N_c^{(f)} e_f^2 \left(\frac{1}{\bar{\epsilon}} - \log\frac{m_f^2}{\mu^2}\right) - \frac{7}{4}\left(\frac{1}{\bar{\epsilon}} - \log\frac{m_W^2}{\mu^2}\right) - \frac{1}{6}\Bigg\}, \end{aligned} \tag{4.24}$$

which we shall use by setting $\mu = m_Z$. While eqs. (4.23) and (4.24) are fully general, we point out that in the SM the "heavy" tag applies only to the top quark.

In order to compute the numerical value of α_{m_Z}, we start by observing that from eq. (4.18) we have:

$$\alpha_{m_Z} = \frac{\alpha(0)}{1 - \Delta\alpha}\,. \tag{4.25}$$

The r.h.s. of this equation can be evaluated by using the Thomson value of eq. (4.16) and the lepton and quark contributions of eqs. (4.20) and (4.21), respectively, obtained from the perturbative result of eq. (4.22). While this procedure is perfectly fine in the case of the leptons, for the quarks it introduces a significant source of uncertainty that stems from

JHEP10(2022)089

the fact that light-quark masses are unphysical parameters. As is well known, this problem can be avoided by using a value of $\Delta\alpha_H^{(5)}$ that is obtained from a dispersion relation fitted to $e^+e^- \to hadrons$ data; from the PDG [34]:

$$\Delta\alpha_H^{(5)} = 0.02766 \pm 0.00007\,. \tag{4.26}$$

We observe that the perturbative result for $\Delta\alpha_H^{(5)}$ stemming from eq. (4.22) is equal to about 0.036 if the masses of eq. (5.1) (i.e. the PDG's central values) are employed. Equation (4.22) would lead to the phenomenologically-sensible result of eq. (4.26) only if the masses of the quarks, and in particular those of the three lightest ones, were assigned much larger values (and generally way outside of the respective uncertainty ranges) w.r.t. to the central ones reported on the PDG; we shall briefly return to this point in section 6.1. By using eq. (4.26) we finally obtain:

$$\alpha_{m_Z} = 1/128.940\,. \tag{4.27}$$

Moreover, eqs. (3.2) and (4.24) can be exploited with the definition of eq. (4.2) to arrive at the following result:

$$\Delta_{\overline{\rm MS}\to\alpha(m_Z)} = \frac{5}{9\pi}\,C^{(2,M)} + \frac{1}{\pi}\left(\frac{7}{4}\log\frac{m_W^2}{m_Z^2} - \frac{1}{6}\right). \tag{4.28}$$

With this, we can evaluate the $\overline{\rm MS}$ coupling constant at $\mu = m_Z$. The analogue of eq. (4.25) reads:

$$\alpha(m_Z) = \frac{\alpha(0)}{1 - \Delta\alpha - \Delta_{\overline{\rm MS}\to\alpha(m_Z)}}\,, \tag{4.29}$$

whence:[15]

$$\alpha(m_Z) = 1/127.955\,. \tag{4.30}$$

We have explicitly verified that, by defining the $\overline{\rm MS}$ scheme without the decoupling of the top quark, we obtain a value for $\alpha(m_Z)$ which is in excellent agreement with that of ref. [35] (whose definition is identical to that stemming from eq. (3.2) except from the role of the top) — the very small residual differences are due to our neglecting two-loop effects.

In the G_μ scheme, we define the renormalisation constant for α thus:

$$Z_{\alpha_{G_\mu}} = Z_{\alpha(0)} - \Delta r\,, \tag{4.31}$$

with (see e.g. ref. [29]):

$$\Delta r = \Pi^{AA}(0) + \Delta r^{(1)}\,, \tag{4.32}$$

$$\begin{aligned}\Delta r^{(1)} = &-\frac{c_W^2}{s_W^2}\left(\frac{\Sigma_T^{ZZ}(m_Z^2)}{m_Z^2} - \frac{\Sigma_T^{W}(m_W^2)}{m_W^2}\right) - \frac{\Sigma_T^{W}(0) - \Sigma_T^{W}(m_W^2)}{m_W^2} \\ &+2\frac{c_W}{s_W}\frac{\Sigma_T^{AZ}(0)}{m_Z^2} + \frac{\alpha}{4\pi s_W^2}\left(6 - \frac{7-4s_W^2}{2s_W^2}\log c_W^2\right),\end{aligned} \tag{4.33}$$

[15] If the W contribution is neglected in eq. (4.28), one obtains a value of $\alpha(m_Z)$ which is 0.15% larger than that in eq. (4.30).

JHEP10(2022)089

where we understand that only the real parts of the two-point functions have to be taken into account. From eq. (4.13) we then obtain:

$$Z_{\alpha_{G_\mu}} = -2\frac{s_W}{c_W}\frac{\Sigma_T^{AZ}(0)}{m_Z^2} + \Delta r^{(1)}\,. \tag{4.34}$$

The numerical value of α_{G_μ} is determined by means of the following relationship:

$$\alpha_{G_\mu} = \frac{\sqrt{2}G_\mu m_W^2\left(m_Z^2 - m_W^2\right)}{\pi m_Z^2} \equiv 1/132.183\,, \tag{4.35}$$

from which, by employing eq. (4.2) and by making use of eq. (4.30), we obtain:

$$\Delta_{\overline{\rm MS}\to G_\mu} = 4.092936\,. \tag{4.36}$$

We remind the reader that Δr is known to receive large contributions beyond one loop. We take this effectively into account by using eqs. (4.35) and (4.36), rather than their one-loop expressions stemming from eqs. (4.31)–(4.33). This is conceptually equivalent to using eq. (4.26) in the $\alpha(m_Z)$ scheme rather than its perturbatively-computed counterpart.

We finally note that the definitions given above are fully consistent with those employed [26] in the $\alpha(m_Z)$ and G_μ UFO models in MG5_aMC.

5 Numerical solution

The numerical approach adopted here is conceptually identical to the one presented in ref. [23]: the evolution of the PDFs is performed by solving the evolution equations in Mellin space, in terms of the evolution operator introduced in section 3.3. The latter, applied to the PDFs evaluated at μ_0 (i.e. to the PDF initial conditions) returns the PDFs at the desired final scale μ.

From the practical viewpoint, however, several changes are required w.r.t. the implementation of ref. [23], owing to the presence of multiple fermion families, as well as to the possibility to adopt different factorisation and renormalisation schemes; more details on this are given in section 5.2.

Moreover, the integrable divergence of the electron PDF at $z = 1$ must be handled with care in the convolution with short-distance cross sections of eq. (1.2), lest the numerical accuracy be degraded. In order to do so, in the region $z \simeq 1$ one switches from the numerical solution to the analytical one found in section 3.3; such a switching is detailed in section 5.3.

The code that implements the numerical solution of the evolution equations and the switching to the analytical solution is described in section 5.4.

5.1 Partonic content

In order to perform the PDF evolution with multiple fermion families according to the discussion at the beginning of section 3 we have employed the so-called variable-flavour-number scheme (VFNS) [36], in which the PDF of each fermion, be it a lepton or a quark, is

JHEP10(2022)089

generated radiatively starting from the corresponding threshold, that we assume to be equal to the mass of the fermion itself. In this scheme, the entire evolution range is subdivided into sub-ranges (see eq. (3.6)) characterised by a specific number of leptons, $n_l \leq N_l$, and quarks, $n_f \leq N_u + N_d$. In each such sub-range, the evolution operator is evaluated as is explained in ref. [23] including only n_l leptons and n_f quarks. Finally, all of the evolution operators thus obtained are consistently matched at thresholds.[16] We have chosen the fermion masses equal to the corresponding central values quoted in the PDG [34], namely:

$$\begin{aligned} m_e &= 0.5109989461 \cdot 10^{-3}\ \text{GeV}\,, \\ m_u &= 2.16 \cdot 10^{-3}\ \text{GeV}\,, \\ m_d &= 4.67 \cdot 10^{-3}\ \text{GeV}\,, \\ m_s &= 0.093\ \text{GeV}\,, \\ m_\mu &= 0.1056583745\ \text{GeV}\,, \\ m_c &= 1.27\ \text{GeV}\,, \\ m_\tau &= 1.77686\ \text{GeV}\,, \\ m_b &= 4.18\ \text{GeV}\,, \end{aligned} \tag{5.1}$$

which are strictly ordered as was assumed in eq. (3.1). We note that, in the case of quark masses, other criteria can be adopted to set their values — one explicit example is given in section 4.1 in the context of the definition of the $\alpha(m_Z)$ UV-renormalisation scheme; we shall also briefly return to this point in section 6.1. Finally, in this paper we set the initial scale for the evolution equal to the electron mass, $\mu_0 = m_e$.

As was already anticipated, we perform the numerical evolution using a slightly different functional basis w.r.t. that introduced in section 3.1: while eqs. (3.9)–(3.16) are employed as such, the eight non-singlet functions of eq. (3.8) are re-combined as follows [37]:

$$\Gamma_{V_l} = \sum_{l=1}^{N_l} \left(\Gamma_l - \Gamma_{\bar{l}}\right), \tag{5.2}$$

$$\Gamma_{V_u} = \sum_{u=1}^{N_u} \left(\Gamma_u - \Gamma_{\bar{u}}\right), \tag{5.3}$$

$$\Gamma_{V_d} = \sum_{d=1}^{N_d} \left(\Gamma_d - \Gamma_{\bar{d}}\right), \tag{5.4}$$

$$\Gamma_{V_1^l} = \Gamma_{e^-} - \Gamma_{e^+} - \left(\Gamma_{\mu^-} - \Gamma_{\mu^+}\right), \tag{5.5}$$

$$\Gamma_{V_2^l} = \Gamma_{e^-} - \Gamma_{e^+} + \Gamma_{\mu^-} - \Gamma_{\mu^+} - 2\left(\Gamma_{\tau^-} - \Gamma_{\tau^+}\right), \tag{5.6}$$

$$\Gamma_{V_1^u} = \Gamma_u - \Gamma_{\bar{u}} - \left(\Gamma_c - \Gamma_{\bar{c}}\right), \tag{5.7}$$

$$\Gamma_{V_1^d} = \Gamma_d - \Gamma_{\bar{d}} - \left(\Gamma_s - \Gamma_{\bar{s}}\right), \tag{5.8}$$

$$\Gamma_{V_2^d} = \Gamma_d - \Gamma_{\bar{d}} + \Gamma_s - \Gamma_{\bar{s}} - 2\left(\Gamma_b - \Gamma_{\bar{b}}\,,\right). \tag{5.9}$$

[16] Up to NLL accuracy and by setting the fermion thresholds equal to the respective masses, the matching implies that radiatively-generated fermions have a vanishing PDF at the respective thresholds. We point out that this is generally not true, and that at orders higher than NLL, or by choosing thresholds different from mass values, radiatively-generated PDFs at threshold are different from zero but perturbatively computable.

JHEP10(2022)089

As was done in eqs. (3.8)–(3.16), these are given for a maximal number of light fermions, and the same comment as in footnote 8 applies here. The reason for using the basis of eqs. (5.2)–(5.9) rather than that of eq. (3.8) is a practical one: our numerical code is built upon an existing one relevant to QCD [38], that can handle NNLL evolution as well: at that order eqs. (5.2)–(5.9) are more convenient than eq. (3.8).[17] Thus, while at the LL and NLL the two bases are equally sensible, the choice made in this section allows us to minimise the changes to the original computer code.

Needless to say, in the numerical code the exact forms of the AP kernels are used, as opposed to the $N \to \infty$ ones employed for the analytical solutions in the $z \to 1$ region. This implies that, in the singlet sector, we solve eq. (3.31) rather than eq. (3.32). Conversely, as in the case of the analytical solutions, when the evolution is carried out at the LL only the first term of the perturbative expansion of each AP kernel, eq. (3.17), is retained, while the flavour structure is exactly the same as for the NLO+NLL solutions. Therefore, contrary to what is typically done in the literature, also at the LO+LL we have non-vanishing photon, positron, and quark PDFs.

5.2 Evolution in Mellin space

The differential equation we solve has the following structure:

$$\frac{\partial \mathbb{E}_N^{(K)}(\mu)}{\partial \log \mu^2} = \mathbb{M}_N^{(K)}(\alpha(\mu), \mu)\, \mathbb{E}_N^{(K)}(\mu)\,, \qquad \mathbb{E}_N^{(K)}(\mu_I) = \mathbb{E}_{I,N}^{(K)}\,, \tag{5.10}$$

where $\mathbb{M}_N^{(K)}$ and $\mathbb{E}_N^{(K)}$ are either 4×4-dimensional matrices in the singlet sector (eq. (3.31)) or scalar functions (all of the other cases). Equation (5.10) is understood to be relevant in the range of eq. (3.49), and μ_I denotes the lower end of that range (i.e. μ_0 or m_k when non-empty), where the evolution operator assumes the value $\mathbb{E}_{I,N}^{(K)}$. We solve eq. (5.10) recursively, starting from the lowest k value for which the range of eq. (3.49) is non-empty, and $\mathbb{E}_{I,N}^{(K)} = I$: in the case we are considering in this paper (the electron PDFs with all thresholds set equal to the respective masses), this implies $k = 1$ and $\mu_0 = m_1 \equiv m$. Then, the value assumed by the evolution operator at the upper end of the range, $\mathbb{E}_N^{(K)}(m_{k+1})$, coincides, by continuity, with the starting value $\mathbb{E}_{I,N}^{(K)}$ relevant to the next range $\mu \in (m_{k+1}, m_{k+2})$. The procedure is thus iterated, which corresponds to the successive determination of the integration constants A_k that appear in eq. (3.54) in the explicit example given for the non-singlet evolution of section 3.3.

The most trivial of cases is that where $\mathbb{M}_N^{(K)}$ does not depend on μ, neither directly nor through $\alpha(\mu)$. This happens in the $\overline{\text{MS}}$ UV-renormalisation scheme when the running of α is neglected. We hasten to stress that this is an unphysical situation (since the coupling constant *does* run in $\overline{\text{MS}}$), that we use solely for testing purposes — we shall comment briefly on this in section 6.3. The solution is given by the following expression:

$$\mathbb{E}_N^{(K)}(\mu) = \exp\left(\mathbb{M}_N^{(K)} \log \frac{\mu^2}{\mu_I^2}\right) \mathbb{E}_{I,N}^{(K)}\,. \tag{5.11}$$

[17] This is because while eqs. (5.5)–(5.9) evolve with P_f^-, eqs. (5.2)–(5.4) evolve with $P_f^- + n_f(P_{ff}^{\text{S}} - P_{f\bar{f}}^{\text{S}})$, and these two kernels coincide only up to $\mathcal{O}(\alpha^2)$.

JHEP10(2022)089

In the singlet sector (4×4 matrices) the r.h.s. of eq. (5.11) cannot be given in a closed form, and we use a series expansion instead, by keeping as many terms as are deemed necessary for targeting a numerical accuracy of a relative 10^{-8} precision.

When $\mathbb{M}_N^{(K)}$ depends on μ only through $\alpha(\mu)$ (in the cases we consider, this corresponds to the $\overline{\text{MS}}$ UV-renormalisation scheme), we first trade the evolution variable μ for t_k, in keeping with section 3.3, and then we adopt a discretised path-ordered product [39], as has been done in ref. [23]. The range of eq. (3.51) is split into "small" n_k sub-intervals, $(t_{0,k}, t_{1,k})$, ... $(t_{n_k-1,k}, t_{n_k,k})$, which for simplicity are evenly spaced:

$$t_{i,k} = t_{0,k} + i\Delta_k t\,, \qquad i = 0,\ldots,n_k\,, \qquad \Delta_k t = \frac{t_{n_k,k} - t_{0,k}}{n_k}\,, \tag{5.12}$$

$$t_{0,k} = 0\,, \tag{5.13}$$

$$t_{n_k,k} = \bar{t}_k\,. \tag{5.14}$$

Then, if $\Delta_k t \ll 1$, the following discretised expression for the evolution operator works fairly well:

$$\mathbb{E}_N^{(K)}(\mu) \simeq \left[\prod_{i=0}^{n_k-1} \exp\left(\frac{\Delta_k t}{2}\left(\mathbb{M}_N^{(K)}\left(t_{i,k}\right) + \mathbb{M}_N^{(K)}\left(t_{i+1,k}\right)\right)\right)\right] \mathbb{E}_{I,N}^{(K)}\,, \tag{5.15}$$

and we adopt it in our computations. We point out that, more in general, the $\Delta_k t \ll 1$ condition allows the usage, as the argument of the exponential in eq. (5.15), of any function of $\mathbb{M}_N^{(K)}$ that depends only on the endpoints $t_{i,k}$ and $t_{i+1,k}$; the differences induced by different choices for this function vanish for $\Delta_k t \to 0$.

It remains to determine how to set the n_k parameters so that the sub-intervals used here are small enough to guarantee that the discretised approach of eq. (5.15) does not degrade the numerical accuracy of the solution. In order to do that, we notice that the larger the number of fermions in the evolution, the slower the convergence of the path-ordered product. This ultimately happens because the evolution is predominantly driven by the running of α, which in turn is controlled by the β-function coefficients, whose values scale linearly with the number of fermions (see eq. (3.7)). As a consequence of that, the total number of sub-intervals $\sum_k n_k$ required to achieve comparably-accurate results in different ranges is expected to scale roughly with the number of fermions, $M = N_l + N_u + N_d$. In view of the fact that it has been heuristically established in ref. [23] that in the case of a single-fermion evolution (i.e. for $N_l = 1$ and $N_u + N_d = 0$), and for the largest scales of the order of the TeV, an appropriate total number of sub-intervals is equal to 20, by making a conservative choice we set

$$\sum_{k=1}^{M} n_k \geq n \equiv 300\,. \tag{5.16}$$

While the individual values of n_k could also be assigned by taking into account the scaling with the number of active fermions, this would ignore the fact that mass thresholds are not evenly spaced. We can take both effects into account with the following settings:

$$n_k = n\,\frac{v(\min(\mu, m_{k+1})) - v(\overline{m}_k)}{v(\mu) - v(\mu_0)}\,, \tag{5.17}$$

JHEP10(2022)089

with $v(x) = \alpha(x)$. As a final refinement, since eq. (5.17) might lead to the undersampling of the ranges defined by two thresholds particularly close to each other, we actually use:

$$n_k \longrightarrow \Theta(n_k) \max\left(n_{\min}, n_k\right) , \qquad n_{\min} = 50 . \tag{5.18}$$

Equations (5.16)–(5.18) have been validated by varying the numerical values that appear therein. We have found that the PDFs are unchanged within the target relative accuracy of 10^{-8} for $200 \le n \le 1000$ and $20 \le n_{\min} \le 300$.

We finally must consider the case where $\mathbb{M}_N^{(K)}$ has a direct dependence on μ, but α does not run — this happens in the $\alpha(m_Z)$ and G_μ schemes. In the non-singlet case, we exploit a closed-form analytical solution, the fixed-α counterpart of eq. (3.54) that can be easily obtained by solving eq. (4.7). In the singlet case, we adopt two different strategies, which are used to validate each other. The first strategy is a path-ordered product analogous to that in eq. (5.15), but with evolution variable

$$L(\mu) = \frac{\alpha}{2\pi} \log \frac{\mu^2}{\mu_I^2} \tag{5.19}$$

instead of t_k, so that $v(x) = L(x)$ in eq. (5.17), with the analogues of the $t_{i,k}$ parameters of eq. (5.12) defined in the space spanned by the values of L. The second strategy is based on a Magnus expansion [40]:

$$\mathbb{E}_N^{(K)}(\mu) = \exp\left(\sum_{i=1}^{\infty} \Omega_i(\mu, \mu_I)\right) \mathbb{E}_{I,N}^{(K)} , \tag{5.20}$$

where for instance the first two terms are given by:

$$\Omega_1(\mu, \mu_I) = \int_{\log \mu_I^2}^{\log \mu^2} d \log \kappa^2 \, \mathbb{M}_N^{(K)}(\kappa) , \tag{5.21}$$

$$\Omega_2(\mu, \mu_I) = \frac{1}{2} \int_{\log \mu_I^2}^{\log \mu^2} d \log \kappa_1^2 \int_{\log \mu_I^2}^{\log \kappa_1^2} d \log \kappa_2^2 \left[\mathbb{M}_N^{(K)}(\kappa_1), \mathbb{M}_N^{(K)}(\kappa_2)\right] . \tag{5.22}$$

We have limited ourselves to considering the first four terms in the series at the exponent in eq. (5.20). Since the running time of the Magnus-expansion-based implementation is shorter than that based on the path-ordered approach, we have adopted the former as our default strategy for the $\alpha(m_Z)$ and G_μ schemes, after having verified that the two strategies give the same PDFs within the target relative accuracy of 10^{-8} (the parameters n and $n_{\min}$ of eqs. (5.16) and (5.18) have been used in the path-ordered case).

Finally, in order to invert the PDFs from the Mellin to the z space we employ the same strategy already used in ref. [23], namely a numerical algorithm based on the so-called Talbot path [41], with a trapezoidal integration.

5.3 Switching to the analytical solution

The numerical approach described so far cannot possibly work in the $z \to 1$ limit, owing to the fact that the electron PDF has a very steep, power-like integrable singularity. In order to address this issue we make use of the analytical solution of section 3.3 to define

JHEP10(2022)089

a PDF which is accurate and well-behaved in the whole z range. Denoting by $\Gamma_{\rm num}$ and $\Gamma_{\rm an}$ the numerical solution and its associated analytical one, respectively, we introduce a switching point z_0, and define the complete solution as follows (generalising what was done in ref. [42]):

$$\Gamma(z) = \begin{cases} \Gamma_{\rm num}(z)\,, & z \le z_0\,, \\ \Gamma_{\rm an}(z)\left(s(z;z_0)\dfrac{\Gamma_{\rm num}(z_0)}{\Gamma_{\rm an}(z_0)} + 1 - s(z;z_0)\right), & z > z_0\,, \end{cases} \tag{5.23}$$

with:

$$s(z;z_0) = \left(\frac{1-z}{1-z_0}\right)^k\,, \qquad k \ge 1\,. \tag{5.24}$$

The factor in round brackets on the r.h.s. of eq. (5.23) is chosen so that $\Gamma(z)$ is continuous at $z = z_0$ and coincides with the analytical solution at $z = 1$. For all practical purposes, this is essentially academic. In fact, the switching point z_0 is chosen in such a way that $\Gamma_{\rm num}(z_0)$ and $\Gamma_{\rm an}(z_0)$ are virtually identical,[18] and the numerical solution $\Gamma_{\rm num}(z_0)$ has not yet lost accuracy. Typical values for z_0 are between $1 - 10^{-6}$ and $1 - 10^{-7}$; for these, we observe that $\Gamma_{\rm num}(z_0)/\Gamma_{\rm an}(z_0) \simeq z_0$. This implies that in practice the choice of k in eq. (5.24) has a negligible impact;[19] in phenomenological applications, we employ $k = 2$.

We remind the reader that in the $\overline{\rm MS}$ renormalisation and factorisation schemes an $\mathcal{O}(\alpha^3)$-accurate analytical solution exists also for $z < 1$ [23] that, matched with the $z \to 1$ one, offers an alternative to the form defined in eq. (5.23). However, such a solution has been derived only for single-lepton evolution, and because of that is not employed here.

5.4 Code EMELA

The strategy described in this section has been implemented in a code that we call EMELA, which we release together with the current paper. Such a code supersedes the one developed in ref. [23] (EPDF), that was limited to the evolution with a single lepton in the $\overline{\rm MS}$ renormalisation and factorisation schemes.

The new code is available at the link: https://github.com/gstagnit/eMELA, where documentation and examples about its usage can also be found. EMELA is a standalone code, and can be linked to any external program.

More in detail, EMELA is an improved QED-version of MELA [38]. It consists of a Fortran code responsible for the numerical evolution of the PDFs, and a C++ wrapper that provides one with the analytical solutions and the switching described in section 5.3. Moreover, since a runtime evaluation of the numerical solution is likely too slow for phenomenological applications, the possibility is given to the user to output the PDFs as grids compliant with the LHAPDF [43] format, that can be employed at a later stage.

We stress that, regardless of whether the numerical solution is computed at runtime or read from the grids, EMELA always switches to the analytical solution at $z = z_0$. Furthermore, in order for the output to be handled within machine-precision double arithmetic for

[18] Which constitutes a powerful consistency check of the numerical and analytical solutions.

[19] More precisely, the relative differences between cross sections obtained with $k = 0$, $k = 1$, and $k = 2$ are at the level of 10^{-6}, i.e. within our MC integration errors.

JHEP10(2022)089

values of z arbitrarily close to one, the code returns the PDFs multiplied by a user-defined damping factor that vanishes at $z \to 1$, following the procedure introduced in section 3 of ref. [27].

The interested reader can find all of the necessary technical information by visiting the link given above. There, one can also find pre-computed grids with different choices of renormalisation scheme, factorisation scheme, and so forth. Such grids are validated, and have been used for the cross section calculations of section 6.

6 Results

In this section we employ the PDFs we have derived as was explained in sects. 3–5 to compute cross sections according to eqs. (1.1) and (1.2). We do so in the automated MG5_aMC framework, thereby extending the simulation of ISR effects in e^+e^- collisions of ref. [27] from LO+LL to NLO+NLL accuracy. As was already mentioned in section 1, this means that MG5_aMC can now also compute NLO EW corrections for processes with massless initial-state leptons; this has required some changes in the implementation of the FKS subtractions relevant to this case — more details can be found in appendix C. We study the processes:

$$e^+e^- \longrightarrow q\bar{q}(\gamma)\,, \tag{6.1}$$

$$e^+e^- \longrightarrow W^+W^-(X)\,, \tag{6.2}$$

$$e^+e^- \longrightarrow t\bar{t}(X)\,, \tag{6.3}$$

at the NLO accuracy (i.e. at $\mathcal{O}(\alpha^3)$), where the symbols in round brackets denote any particle that may be present in the final state beyond the LO. In eq. (6.1) q is a massless fermion of charge e_q, and in the corresponding short-distance cross sections we retain only the contributions proportional to e_q^2 — this is therefore the process already used in ref. [22] (the constraint on the quark charge being specified in eq. (4.3) there; this limits the real and virtual radiation to the initial state, and thus the process is effectively equivalent to that for the production of a heavy neutral object of variable mass), whose simple analytical cross sections we have used as a cross-check of the corresponding automated computation carried out by MG5_aMC. The results for the processes of eqs. (6.2) and (6.3) include EW contributions to the short-distance cross sections. The latter case is also computed as a pure-QED process, i.e. by ignoring EW effects. The process of eq. (6.1) is always dealt with in QED.

Beam-dynamics effects, parametrised by the functions $\mathcal{B}_{kl}(y_+, y_-)$ of eqs. (1.1) and (2.1), are generally ignored; when included, we restrict ourselves to considering a single illustrative case (a 500-GeV collider with an ILC-type configuration), where such effects are implemented as is detailed in ref. [27]; we discuss it in section 6.5.

The aim of this section is to document the effects of the theoretical novelties introduced here and in refs. [22–24] on actual observables; in order to keep the number of plots at a manageable level, we present results for the cumulative cross section:

$$\sigma(\tau_{\min}) = \int d\sigma\, \Theta\left(\tau_{\min} \le \frac{M^2_{p\bar{p}}}{s}\right), \qquad p = q\,, t\,, W^+\,, \tag{6.4}$$

JHEP10(2022)089

where $M^2_{p\bar{p}}$ is the invariant mass squared of the $p\bar{p}$ pair, and s the collider c.m. energy squared. We employ MG5_aMC to compute this observable at fixed order, either leading or next-to-leading; in other words, soft logarithms that appear at $\tau_{\rm min} \to 1$ are not resummed. We stress that MG5_aMC is capable of computing simultaneously any number of observables, subject to arbitrary final-state cuts. Our primary interest is the assessment of the impact of NLL contributions to the PDFs, and of the factorisation- and renormalisation-scheme dependencies, which we shall discuss in sects. 6.2 and 6.3, respectively. In order to do so in a manner conceptually analogous to what is typically done in the literature, in those sections we shall limit ourselves to including only the e^+e^--initiated *partonic* channel results. The contributions of other partonic channels that enter eqs. (6.2) and (6.3), and in particular the $\gamma\gamma$ one, will be discussed in section 6.4 (see also section 6.1). We typically consider all of the six possible combinations of factorisation (Δ, $\overline{\rm MS}$) and renormalisation ($\overline{\rm MS}$, $\alpha(m_Z)$, G_μ) schemes, except for $q\bar{q}$ and $t\bar{t}$ production in QED, in which cases no results are given for the G_μ renormalisation scheme.

We set the hard scale as follows:

$$\mu = \sqrt{s}\,, \tag{6.5}$$

and employ

$$m_W = 80.379 \text{ GeV}\,, \tag{6.6}$$
$$m_Z = 91.1876 \text{ GeV}\,, \tag{6.7}$$
$$m_t = 173.3 \text{ GeV}\,. \tag{6.8}$$

We present predictions obtained with a $\sqrt{s} = 500\,\text{GeV}$ c.m. energy, but we stress that we have considered (if above the respective pair-production thresholds) several other cases in the range 50 GeV $\leq \sqrt{s} <$ 500 GeV, finding quantitatively similar results. In the legends of the plots, we shall typically employ the following naming conventions:

$$\text{xsec}\,,\ \text{PDF}\ [\text{fact sch}\,,\text{ren sch}]\,, \tag{6.9}$$

where "xsec" denotes the perturbative accuracy of the short-distance cross sections, "PDF" the logarithmic accuracy of the PDFs, and "fact sch" and "ren sch" the factorisation and renormalisation schemes, respectively, used in the latter. Thus:

$$\text{xsec} \in \{\text{LO}\,,\text{NLO}\}\,, \tag{6.10}$$
$$\text{PDF} \in \{\text{LL}\,,\text{NLL}\}\,, \tag{6.11}$$
$$\text{fact sch} \in \{\Delta\,,\overline{\text{MS}}\}\,, \tag{6.12}$$
$$\text{ren sch} \in \{\overline{\text{MS}}\,,\alpha(m_Z)\,,G_\mu\}\,. \tag{6.13}$$

The factorisation-scheme tag is absent when the corresponding PDFs are evaluated at the LL accuracy.

Before going into the details, in section 6.1 we discuss some general features that inform the predictions shown later, and that may be used in the future for further phenomenological refinements.

JHEP10(2022)089

6.1 General considerations and the role of the W

We start by reminding the reader that the requirement that the evolution of α be phenomenologically sensible is the main motivation for employing all fermion families, and their respective mass thresholds, as opposed to limiting oneself to consider only the electron (see section 2). The very same requirement, then, demands that the contribution of the W to the running of α be included as well, since its effect is numerically significant at large scales. For example, the values of $\alpha(\mu)$ at $\mu = 500\,\text{GeV}$ obtained by including or by ignoring the contribution of the W, and computed according to the procedure outlined in section 4.1 with consistent initial conditions at $\mu = m_Z$ (see footnote 15), differ from one another by 1.7% (at one loop); the evolution that includes the W is slower w.r.t. that which excludes it, owing to the negative sign in front of the second term on the r.h.s. of eq. (3.7).

In view of what was said above, the results presented here are obtained by including the W contribution to the running of α; we stress, however, that if one were interested in treating such a contribution as a systematics, EMELA allows one to switch it on and off easily. We note that from the technical viewpoint the inclusion of the W does not pose any problems — the W mass can simply be regarded as an additional threshold, and treated in the same manner as its fermionic counterparts as is explained in sects. 3 and 5. However, we also remark that by doing so we introduce two sources of inconsistency in our framework. Firstly, the W contribution to the running of α is included only at the one-loop level, while pure-QED effects are included up to two loops (see eq. (3.7)). Secondly, by considering weak contributions to the running of α one would need to do the same in the PDF evolution equations, that in turn would entail the necessity of considering branching processes that involve weak bosons, as well as treating weak bosons as partons. We believe that in practice we can safely neglect both of these items. As far as the first one is concerned, heuristic evidence is given by the fact that the changes in the PDFs stemming from very large changes to the $b_1^{(M)}$ coefficient w.r.t. to its value of eq. (3.7) — i.e. setting it equal to zero or doubling it — are very small in absolute value, and completely negligible w.r.t. other theoretical systematics considered here. For what concerns the second item, it should be clear that the large masses of the weak bosons prevent them from giving noticeable contributions even at energies of the order of 1 TeV — the case of *hadronic* PDFs, where analogous kinematic considerations apply, has been explicitly considered, see e.g. refs. [44–46]. Having said that, we stress that the language adopted here gives one a blueprint for the inclusion of the weak bosons in PDF evolution that does not necessitate any conceptual changes, should the need for doing so arise in the distant future.

A potential source of systematics that is ignored as such in this paper is the dependence on the starting scale for the PDF evolution, μ_0, that we always set equal to the electron mass. Still, we point out that the NLO initial conditions do depend, explicitly and implicitly through the coupling constant, on μ_0 (see eqs. (3.41)–(3.43)). In particular, we remark that the presence of $\log \mu_0$ terms in the NLO initial conditions is such that it compensates an analogous dependence stemming from the evolution, so that at the NLO any physical cross section is μ_0-independent. This property does *not* hold true if an NLO short-distance

JHEP10(2022)089

cross section is convoluted with LO+LL PDFs, since the latter have μ_0-independent initial conditions, but μ_0-dependent evolution. There are two solutions for this issue: either one simply understands $\mu_0 = m$ in an LL evolution, as is typically done in the literature; or one compensates for the μ_0 dependence by including a contribution to the NLO short-distance cross section that is engineered to cancel it — this is explained in more detail in appendix A. Irrespective of which of these two solutions one adopts, it is true that a $\log \mu_0$ dependence remains at the NNLO and beyond; this is the ultimate reason that informs the setting $\mu_0 = m$.[20]

Whether the choice of the light-quark masses should be considered a systematics is debatable; these are not physical parameters, and can also be regarded as quantities to be fitted in order to optimise predictions for a given set of observables. For the phenomenological results of this paper we set them equal to the central values reported by the PDG, as is shown in eq. (5.1); here, we limit ourselves to a few comments on the role they play in the PDFs. Firstly, we stress that the in coupling-constant evolution that we carry out as is explained in section 3 the presence of multiple fermion families and their respective mass thresholds set according to eq. (5.1) is such that $\alpha(m) = 1/138.290$. This value differs by only 0.9% from the Thomson constant of eq. (4.16). While there is no reason why $\alpha(m)$ and the Thomson value should coincide, it appears to be phenomenologically sensible that they are close to each other.[21] Secondly, it has been observed in section 4.1 that a value of $\Delta\alpha_H^{(5)}$ close to that of eq. (4.26) can be obtained by means of a perturbative calculation by employing relatively large values of the light-quark masses. For example, by setting the masses of the three lightest quarks equal to the muon mass, we obtain $\alpha(m) = 1/136.956$ (and $\Delta\alpha_H^{(5)} = 0.0266$), which differs from the Thomson value by a mere 0.06%. Therefore, one can argue that such a choice is better motivated from a phenomenological viewpoint than that of eq. (5.1). While this remains to be seen, and will not be investigated any further in this paper, we observe the following: the $\mathcal{O}(1\%)$ difference in the values of $\alpha(m)$ obtained with eq. (5.1) and with the choice discussed above does *not* lead to a difference of $\mathcal{O}(1\%)$ between the PDFs evolved with these two choices of quark masses — e.g. for the electron PDFs at the NLL, and for scales of $\mathcal{O}(10$ GeV) or larger, the difference is in fact below the permille level.[22] In other words, the $\mathcal{O}(1\%)$ difference in the initial condition is compensated by the different "speeds" in the evolution in the relevant mass ranges.

We also remind the reader that for PDFs beyond the LL the identity of the parton (index i or j in eq. (1.2)) and of the particle (index k or l in eq. (1.2)) need not coincide.[23] When this happens (as is schematically depicted on in the l.h.s. panel of figure 1 for an electron particle) one generally obtains a contribution which is larger than those relevant to all of the other cases (in the r.h.s. panel of figure 1 we depict the most relevant among

[20] We remark that analogous considerations hold for mass thresholds.

[21] For comparison, the evolution with all fermions kept active down to the electron mass leads to $\alpha(m) = 1/144.983$.

[22] And totally negligible for $\alpha(\mu)$ itself, which for large scales is primarily constrained by eq. (4.30) and by the fact that there all fermions are active in the evolution.

[23] At the LO+LL whether non-zero PDFs with $i \neq k$ exist is a matter of conventions. While we do consider them, as opposed to the standard approach in the literature that ignores them, in practice their contributions are minuscule. See also section 6.4.

JHEP10(2022)089

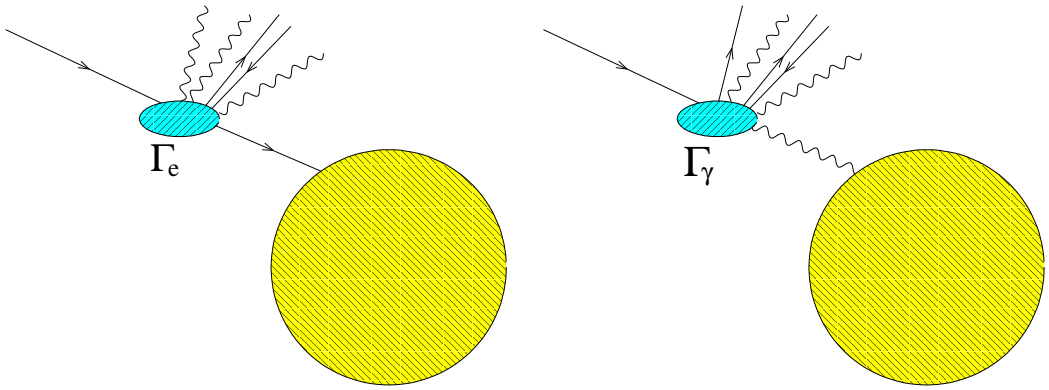

Figure 1. Electron (left panel) and photon (right panel) PDFs (blue ellipses) in an electron. The full yellow circle represents a generic short-distance process.

them, namely that of the photon PDF). Whether this dominance is also seen at the level of physical cross sections depends ultimately on the short-distance cross sections ($d\hat{\sigma}_{ij}$ in eq. (1.2)), and on the observables one is interested in. As an example which involves the photon PDF we remark that already at the LO (i.e. at $\mathcal{O}(\alpha^2)$) the processes of eqs. (6.2) and (6.3) receive contributions from both of the following partonic production channels:

$$e^+e^- \longrightarrow W^+W^-\,, \qquad e^+e^- \longrightarrow t\bar{t}\,, \tag{6.14}$$

and

$$\gamma\gamma \longrightarrow W^+W^-\,, \qquad \gamma\gamma \longrightarrow t\bar{t}\,. \tag{6.15}$$

Since the photon PDF is of relative $\mathcal{O}(\alpha)$ w.r.t. the electron PDF, one may be tempted to conclude that for physical observables the partonic processes of eq. (6.15) will contribute to NNLO, and can therefore be discarded given that our results are NLO accurate. However, this argument, based strictly on a perturbative expansion of the PDFs, is plain wrong from a phenomenological viewpoint. In fact, we point out that the photon PDF becomes larger than the electron PDF[24] as one moves towards small z values (see ref. [23]), which is a region that can be accessed when the invariant mass of the system produced in the hard collision is much smaller than the available c.m. energy. We shall return to this point in section 6.4. We also observe that quark-initiated contributions to W^+W^- and $t\bar{t}$ production exist as well in the context of a treatment that features multiple fermion families, as the one presented in this paper; we neglect them here.

We finally point out that a soft non-collinear logarithm is exponentiated in the fixed-α LO+LL PDFs which have often been used in the literature.[25] While it is not difficult to arrive at a similar exponentiation in the case of either running-α LO+LL PDFs [13, 16, 47] or (in a naive manner) NLO+NLL PDFs, we have not done it in this paper, since this matter deserves a more thorough analysis. Therefore, for consistency reasons and because our present priority is that of assessing various aspects of collinear physics, such

[24] In spite of it still being perturbatively suppressed by an α factor w.r.t. the electron PDF. In other words, higher-order contributions, that stem from the evolution, do matter.

[25] In eqs. (A.15)–(A.17) neglecting such a logarithm corresponds to setting $\beta_E = e_e^2\eta$.

JHEP10(2022)089

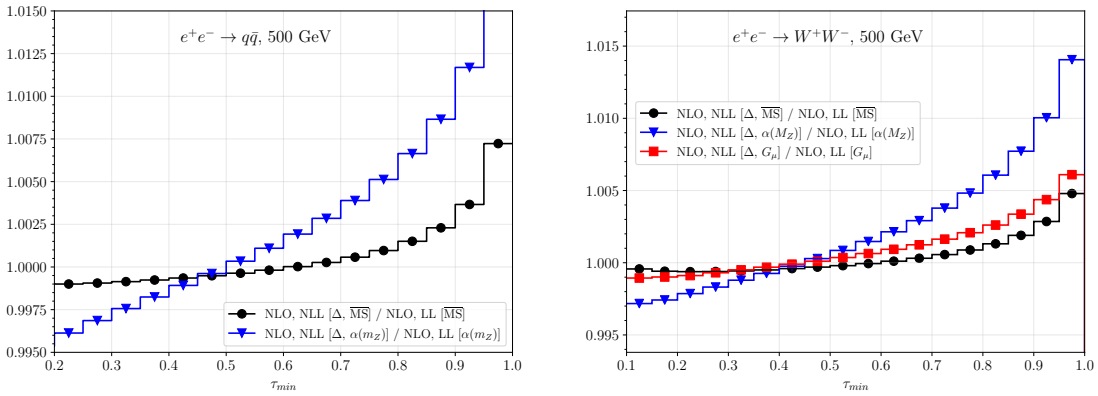

Figure 2. Ratios of NLO cross sections computed with NLL-Δ PDFs over those computed with LL PDFs, for different choices of renormalisation scheme. Left panel: $q\bar{q}$ production; right panel: W^+W^- production.

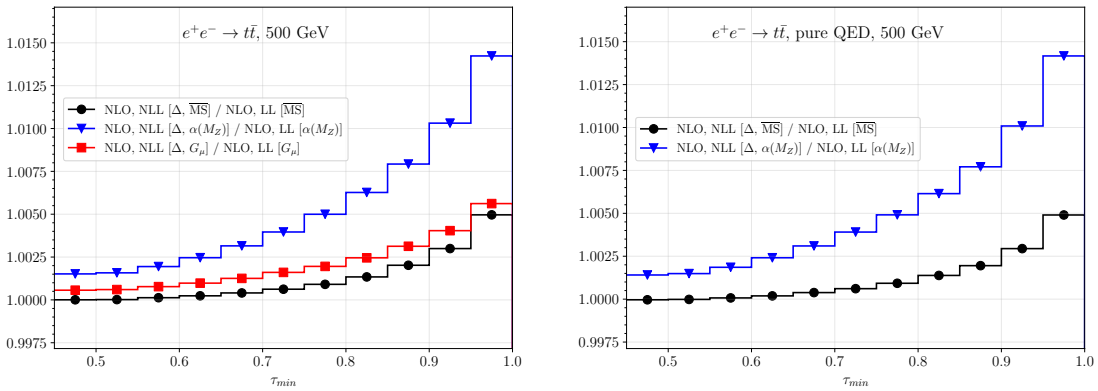

Figure 3. As in figure 2, for $t\bar{t}$ production in the full SM (left panel) and in QED (right panel).

an exponentiated logarithmic term is not included in the LO+LL PDFs we use in the following; thus, for these PDFs we employ either the running scheme (eq. (A.19), in the case of $\overline{\text{MS}}$) or the collinear scheme (eq. (A.18), in the cases of $\alpha(m_Z)$ or G_μ).

6.2 Impact of NLL effects

We start by discussing the impact of the inclusion of the NLL terms in the PDFs. We do so by plotting, in figures 2 and 3, the ratio of the cross section of eq. (6.4) computed (at the NLO) with the NLO+NLL PDFs defined in the Δ factorisation scheme over the same quantity computed with LO+LL PDFs (for the latter ones, either the running or the collinear scheme is employed — see the comment at the very end of section 6.1). We do so for different values of τ_{min}, the results of each of which are represented as bin entries in a histogram.[26] We carry out the computations in the three renormalisation schemes

[26]The ranges in τ_{min} cover all of the kinematically-accessible values; the leftmost bin that we include contains the threshold value $\tau_{\text{min}} = 4m_p^2/s$, except in the case of $q\bar{q}$ production (whose threshold value $\tau_{\text{min}} = 0$ coincides with a singularity of the matrix elements), where we consider $\tau_{\text{min}} \geq 0.2$.

JHEP10(2022)089

considered in this paper, using the same scheme in the numerator and denominator: $\overline{\text{MS}}$ (black curves overlaid with circles), $\alpha(m_Z)$ (blue curves overlaid with triangles), and G_μ (red curves overlaid with boxes). Figure 2 presents the predictions for $q\bar{q}$ production (left panel) and W^+W^- production (right panel), whereas figure 3 is relevant to $t\bar{t}$ production, in the full SM (left panel) and in QED (right panel).

There are a couple of immediate conclusions that can be drawn from the inspection of the figures. Firstly, the relative impact of the NLL contributions can be much larger than the typical precision targets at future e^+e^- colliders, and depends on both the process and the kinematical region one considers (since the histograms are not flat); and, secondly, the dependence on the renormalisation scheme is significant (conversely, we shall show in section 6.3 that the one stemming from the factorisation scheme is much smaller, which is the reason why we could concentrate here on Δ-scheme results). As far as the former aspect is concerned, it is representative of a process- and observable-dependent pattern[27] that renders it impossible to account for NLL PDF effects in some "universal" manner (e.g., with the multiplication of LL-accurate results by an overall factor). Thus, the key conclusion is the following: while the assessment of the relevance of NLL PDF effects depends on the specific applications one pursues (in particular, the observable one considers and the accuracy with which this is expected to be determined experimentally), one should expect them to be phenomenologically important in high-energy e^+e^- collisions, and thus regard NLL-accurate PDFs as the default choice for precision studies in that context.

6.3 Factorisation- and renormalisation-scheme dependences

In this section we consider the dependence of the observable of eq. (6.4) upon the choice of the factorisation and the renormalisation schemes. We first point out that these two dependencies *may* be seen as being of a different nature, in spite of the fact that they both induce differences that are beyond the accuracy one is working at (thus, in our case, the differences are of NNLO). In particular, it is often the case that a definite renormalisation scheme is chosen because it is thought to be particularly apt at correctly capturing dominant effects of perturbative orders higher than those included in the computation one is performing (e.g., the G_μ scheme for processes that involve W's and Z's, and no photons). This viewpoint is of course legitimate, but its validity diminishes with the ability to carry out computations of increasingly-high perturbative accuracy; in such a situation, it is more sensible to regard the differences in predictions stemming from different renormalisation schemes as a theoretical systematics. Conversely, one observes that a factorisation scheme is not defined in relation to some physical property, as is the case for (most of) the renormalisation scheme(s): it is a purely theoretical artifact, in that it defines the finite part of the residue in the subtraction of a collinear singularity. As such, the differences between the predictions obtained with different factorisation schemes are almost by definition a theoretical systematics, although some schemes can be better than others in terms of giving

[27] For each process, we have computed several differential and cumulative observables, and studied them in the same manner as what is done here for that of eq. (6.4).

JHEP10(2022)089

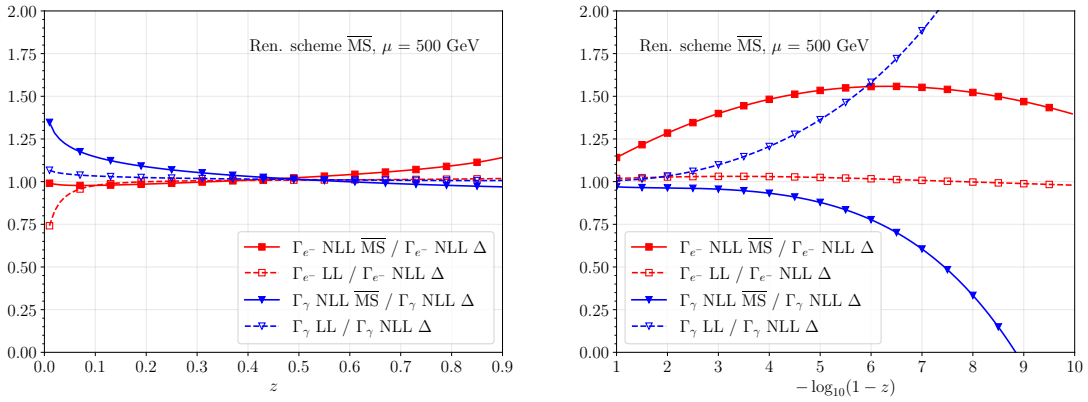

Figure 4. Ratios of NLL $\overline{\text{MS}}$ PDFs (solid curves) and LL PDFs (dashed curves) over NLL Δ PDFs, for an electron (red curves overlaid with boxes) and a photon (blue curves overlaid with triangles); all of the PDFs are computed in the $\overline{\text{MS}}$ renormalisation scheme. The ratios are shown for small- and intermediate-z (left panel), and for $z \simeq 1$ (right panel).

predictions more in line with higher order calculations.[28] And yet, when increasing the perturbative accuracy of the computation such a systematics may become the dominant source of uncertainty, and one may want to find theoretical motivations for a definite choice of the factorisation scheme. While we do not adopt this attitude here (also in view of the fact that we work at the NLO), we point out that the $\overline{\text{MS}}$ and Δ schemes are dramatically different in the $z \simeq 1$ (i.e. the soft) region, and this has some practical consequences.

In order to further the previous point, we must bear in mind that while physical predictions are factorisation-scheme dependent only beyond the perturbative accuracy one is working at, this is not true for either the PDFs or the short-distance cross sections. In the case of the PDFs this is apparent from figure 4. There, we show the ratios of the NLL PDFs computed in the $\overline{\text{MS}}$ factorisation scheme over those computed in the Δ scheme — for both, the $\overline{\text{MS}}$ renormalisation scheme is adopted to be definite (the results in other renormalisation schemes are totally analogous). The results for the electron (red solid curves overlaid with boxes) and photon (blue solid curves overlaid with triangles) PDFs are presented, in the small- and intermediate z region (left panel), as well as for $z \simeq 1$ (right panel). The ratios are extremely large ($\mathcal{O}(1)$ deviations w.r.t. one) in the large-z region, which is particularly significant for the electron, since that region gives by far the dominant contribution to physical observables. For comparison, analogous ratios where the numerators are the LL-accurate PDFs (dashed lines overlaid with boxes and triangles for the electron and the photon, respectively) show deviations from one only of approximately $\mathcal{O}(3\%)$ in the case of the electron (except for very small z values). In other words, NLL PDFs defined in the Δ scheme are quite similar to the LL ones, while very large differences are seen in the case of the $\overline{\text{MS}}$ scheme.

Given the significant differences between the PDFs defined in the $\overline{\text{MS}}$ and Δ schemes, it is remarkable how well the predictions that stem from them agree with each other at the

[28] In the language of the FKS subtraction that is used here, where factorisation schemes are defined by the choices of the $K_{ij}(z)$ functions, it is particularly easy to see how the cancellation of the effects they induce occurs in perturbation theory — see e.g. eq. (B.2) and the comments that follow it.

JHEP10(2022)089

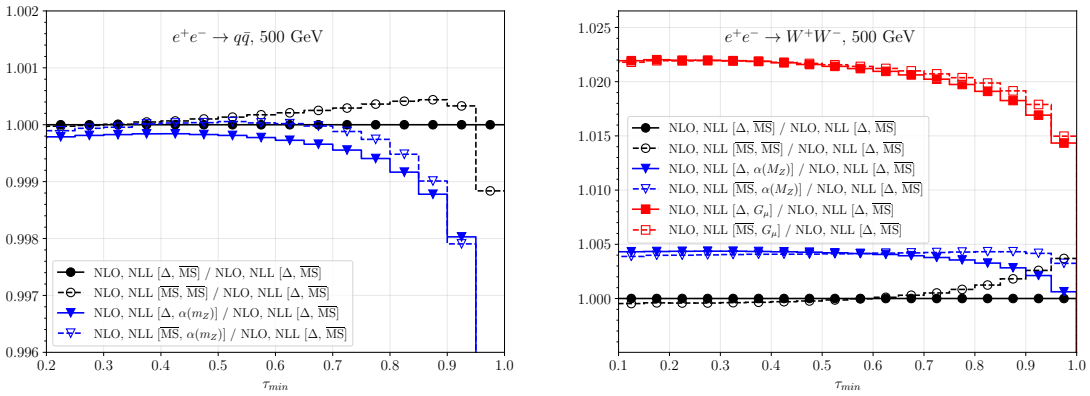

Figure 5. Ratios of cross sections computed with NLL PDFs for all possible combinations of renormalisation and factorisation schemes, over those computed with NLL-Δ PDFs in the $\overline{\text{MS}}$ renormalisation scheme. Left panel: $q\bar{q}$ production; right panel: W^+W^- production.

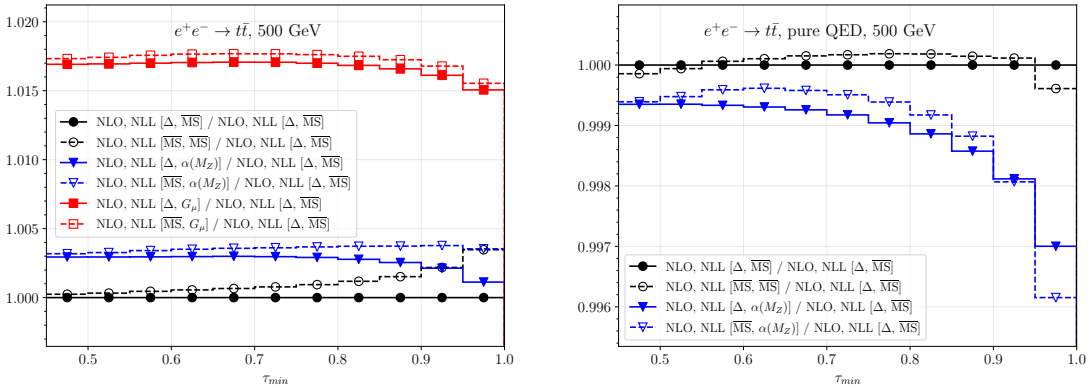

Figure 6. As in figure 5, for $t\bar{t}$ production in the full SM (left panel) and in QED (right panel).

level of observables. This is shown in figures 5–8, which we now comment in some detail. In figure 5 (relevant to $q\bar{q}$ and W^+W^- production) and figure 6 (relevant to $t\bar{t}$ production in the full SM and in QED) we plot the ratios of the NLO results obtained with all of the six combinations of renormalisation and factorisation schemes (four for pure-QED processes, the G_μ scheme being not relevant there), over those obtained by using PDFs defined in the Δ factorisation scheme and in the $\overline{\text{MS}}$ renormalisation scheme. The three solid histograms are those associated with using, in the numerators, PDFs defined in the Δ factorisation scheme and the three renormalisation schemes — $\overline{\text{MS}}$ (black curves overlaid with circles), $\alpha(m_Z)$ (blue curves overlaid with triangles), and G_μ (red curves overlaid with boxes). The three dashed histograms, that employ the same patterns as their solid counterparts, are obtained by using in the numerators PDFs defined in the $\overline{\text{MS}}$ factorisation scheme. Thus, for a given colour/symbol (i.e. a renormalisation-scheme choice) the differences between the solid and dashed histograms measure the factorisation-scheme dependences; whereas for a given pattern (solid or dashed, i.e. a factorisation-scheme choice) the differences among the three colours/symbols measure the renormalisation-scheme dependences.

JHEP10(2022)089

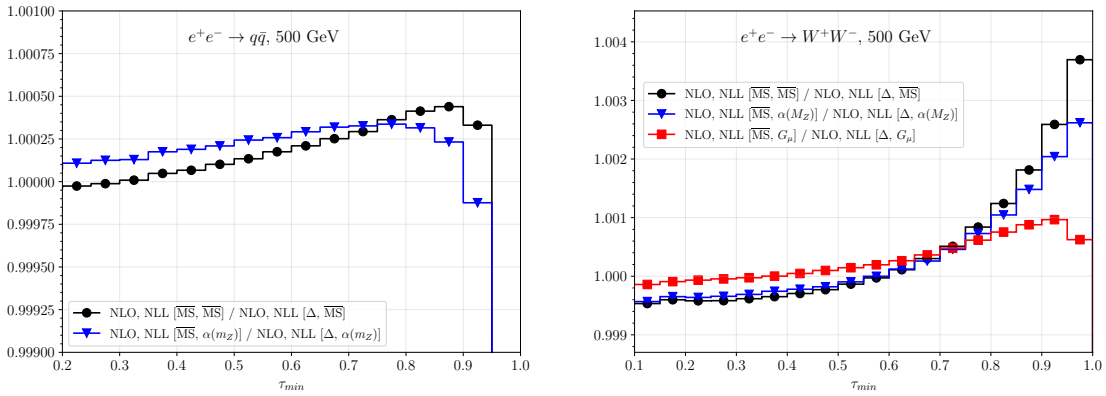

Figure 7. Ratios of cross sections computed with NLL-$\overline{\text{MS}}$ PDFs over those computed with NLL-Δ PDFs, for different choices of renormalisation scheme. Left panel: $q\bar{q}$ production; right panel: W^+W^- production.

The message that emerges in a clear manner is that the renormalisation-scheme dependence is significantly larger than the factorisation-scheme one;[29] this is true independently of the process considered. Note that this behaviour is consistent with the general observations made at the beginning of this section regarding the different nature of theoretical systematics stemming from factorisation- and renormalisation-scheme choices. With that being said, we remark that the renormalisation-scheme dependence is mostly (the exception being again the large-τ_{min} region) a normalisation effect. This is related to the observation, made immediately before section 4.1, that the parameters that control the electron PDF shape at $z \to 1$ ($\xi_1^{(k)}$ and $\hat{\xi}_1^{(k)}$) differ, across the three UV schemes considered here, by terms of $\mathcal{O}(\alpha^3)$, which are thus proven to be not significant numerically. From the previous discussion, however, we expect shape, and not only normalisation, differences to become more relevant with increasing c.m. energy. We have also verified that shape differences are already present at $\sqrt{s} = 500\,\text{GeV}$ if one naively switches the running of α off in $\overline{\text{MS}}$; this underscores our findings that such an unphysical case induces differences of $\mathcal{O}(\alpha^2)$ in the $\xi_1^{(k)}$ and $\hat{\xi}_1^{(k)}$ parameters w.r.t. the actual $\overline{\text{MS}}$ ones, and confirms that with NLL PDFs simply ignoring the running of α in $\overline{\text{MS}}$ is not a viable option for physics simulations: a fixed-α renormalisation scheme, such as $\alpha(m_Z)$ and G_μ, must be used instead.

Another key conclusion from figures 5 and 6 is that these figures show definitely what has been anticipated above, namely that the very significant differences between the NLL PDFs defined in different factorisation schemes do *not* result in large differences at the level of observables: there is a large compensation mechanism at play between the PDFs and the short-distance cross sections.

In order to document the latter remark in a more quantitative manner, in figure 7 (relevant to $q\bar{q}$ and W^+W^- production) and figure 8 (relevant to $t\bar{t}$ production in the full SM and in QED) we present the ratios for our observable obtained by using PDFs defined

[29] One sees a (process-dependent) breakdown of this pattern when $\tau_{\text{min}} \to 1$; we remind the reader that fixed-order predictions lose validity in that region, owing to the emergence of soft unresummed logarithms.

JHEP10(2022)089

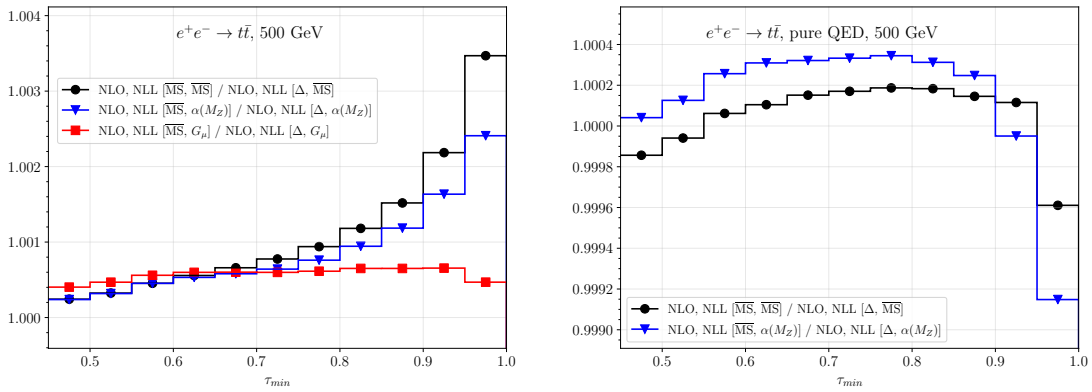

Figure 8. As in figure 7, for $t\bar{t}$ production in the full SM (left panel) and in QED (right panel).

in the $\overline{\text{MS}}$ (Δ) factorisation scheme in the numerator (denominator). We do so separately for the three renormalisation schemes, i.e. $\overline{\text{MS}}$ (black curves overlaid with circles), $\alpha(m_Z)$ (blue curves overlaid with triangles), and G_μ (red curves overlaid with boxes). Thus, for any given colour/symbol, these histograms correspond to the ratios of the dashed over solid histograms with the same patterns that appear in figures 5 and 6. We conclude that the $\mathcal{O}(1)$ differences between different factorisation schemes observed in the PDFs result in $\mathcal{O}(10^{-4} - 10^{-3})$ differences for this observable. While this conclusion holds true irrespective of the process one considers, we point out that the best agreement between the results in the two factorisation schemes is observed for $q\bar{q}$ and $t\bar{t}$ production computed in QED. This is because these processes have a K-factor which is closer to one than that of the full-SM ones — this is shown in figures 12 and 13 (we stress that K-factors are unphysical quantities; the definition we have adopted emphasises the role of the matrix elements, and is largely independent of the PDF choice; see appendix B for more details). The farther away from one the K-factor, the larger the relative impact of matrix elements of NLO ($\mathcal{O}(\alpha^3)$ here) w.r.t. LO ($\mathcal{O}(\alpha^2)$ here) ones; and NLO matrix elements, when convoluted with PDFs, induce a factorisation-scheme dependence of NNLO. Thus, such scheme-dependent NNLO terms are larger for processes with K-factors that differ from one by larger amounts.

A second conclusion to be drawn from figures 7 and 8 can be reached by considering the cancellation of the factorisation-scheme dependence at the NLO. It turns out that in computations performed in $\overline{\text{MS}}$ double-logarithmic terms appear in both the PDFs and in the short-distance cross sections (see the discussion in appendix B), which mutually cancel in the convolution between these quantities. Conversely, such terms are simply not present in the Δ scheme. The implication is that, from the numerical point of view, computations carried out in the $\overline{\text{MS}}$ scheme require a much larger amount of CPU time w.r.t. those performed in the Δ scheme, in order to obtain the same statistical accuracy as the latter ones — this larger CPU footprint is clearly due to the loss of precision that cancellations among large terms entail. In fact, by looking at figure 4, and in particular at the fact that NLL PDFs defined in the Δ ($\overline{\text{MS}}$) factorisation scheme are very close (very different) from the LL ones, one heuristically understands that Δ-based NLO+NLL computations are expected, from a statistical viewpoint, to behave similarly to their NLO+LL analogues.

JHEP10(2022)089

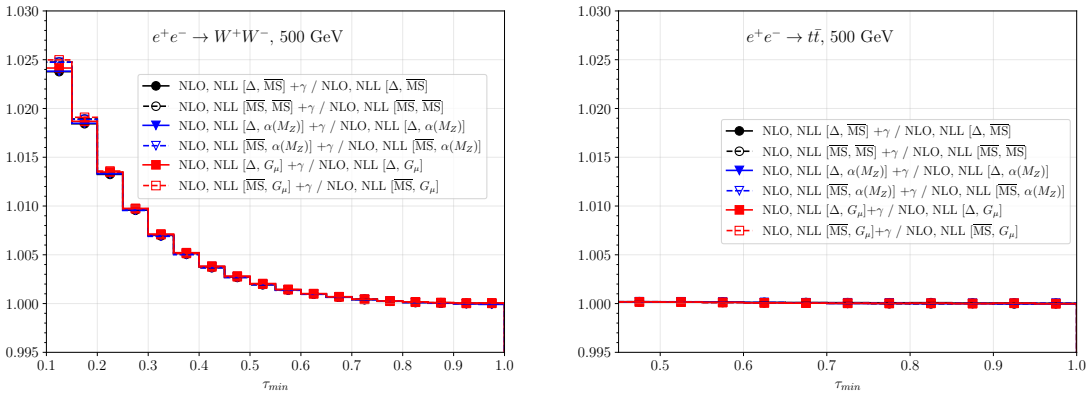

Figure 9. Ratios of cross sections computed by including photon-initiated partonic contributions over their counterparts computed by discarding such contributions, for all possible combinations of renormalisation and factorisation schemes. Left panel: W^+W^- production; right panel: $t\bar{t}$ production in the full SM.

6.4 Impact of photon-induced contributions

As was mentioned at the beginning of section 6, the results of sects. 6.2 and 6.3 have been obtained by keeping only the contributions due to the e^+e^- partonic channels, which are expected to be largely dominant. Still, the master collinear factorisation formula, eq. (1.2), in principle requires an incoherent sum (indices i and j on the r.h.s.) to be performed over all possible partonic channels. Given that our PDFs include $N_l = 3$ leptons, $N_u + N_d = 5$ quarks, and the photon, there are up to $(N_l + N_u + N_d + 1)^2$ channels to be considered. While in QED (at variance with QCD) the well-defined perturbative expansion of the PDFs allows one to formally establish an α-based hierarchy among the contributions due to the above partonic channels, this can be misleading sometimes; for example, this happens when all-order effects significantly modify the PDFs w.r.t. their expressions obtained with a perturbative expansion at some fixed order.

The most interesting case is that of the photon, since its PDF is only suppressed by one power of α w.r.t. that of the electron (all of the other partons have an $\mathcal{O}(\alpha^2)$ suppression). A preliminary discussion on this case has already been given in the final part of section 6.1; here, we aim to study the impact of photon-initiated partonic channels in a couple of explicit cases, namely for W^+W^- and $t\bar{t}$ production in the full SM. In particular, we compare the results one obtains by retaining only the e^+e^- partonic channels with those obtained by including photon-initiated ones as well — at the LO for the two processes considered here, these are eqs. (6.14) and (6.15).[30] Our predictions are presented in figure 9, in the forms of ratios of cross sections obtained with all electron- and photon-initiated partonic channels over those relevant to electron-only channels. All of the six combinations of factorisation- and renormalisation-scheme choices have been considered. The difference between the two processes is striking (this is emphasised graphically by the choice of the same range on

[30] We stress that at the NLO the partonic structure is richer — our results include contributions from all of the possible photon/electron/positron partonic combinations, e.g. $e^+\gamma \to W^+W^-e^+$ and $\gamma\gamma \to W^+W^-\gamma$.

JHEP10(2022)089

the y axis for the two panels of the figure): while for $t\bar{t}$ production the relative impact of the photonic channels is of $\mathcal{O}(10^{-4})$, i.e. within factorisation- and renormalisation-scheme uncertainty, for W^+W^- production at small $\tau_{\rm min}$ (i.e. when the cross section approaches its fully-inclusive value) it is of $\mathcal{O}(1\%)$, larger than any theoretical systematics at this order: it thus represents a physical effect. We note that, at the fully differential level, in regions dominated by small pair invariant masses, the photon-induced contributions can actually be in excess of 50% of the total. Needless to say, a key point here is the process dependence of the results: channels different from the e^+e^- one may or may not give sizable contributions, with a definite answer to be obtained only with specific running conditions and selection cuts. It is therefore important that the PDFs have the ability to include all partonic channels prescribed by the factorisation theorem.

Before concluding this section, a couple of general remarks are in order. Firstly, we remind the reader that the photon PDF is *not* equal to the Weizsaecker-Williams function [48, 49] (WW henceforth); while at $\mathcal{O}(\alpha)$ these two quantities are relatively close to each other (but do not coincide — see e.g. ref. [22]), this is not the case for the all-order PDF vs the WW function. This may induce visible discrepancies between predictions obtained with the photon PDF and the WW function. We also point out that PDFs automatically include a unitarity condition: in other words, when summing over all possible branching types that underpin PDF evolution, the number of incoming particles (the electron in this case) is conserved, so that the fraction of electron- vs photon-initiated partonic processes is the one correctly determined by QED. This is not the case if the LL electron PDF (in particular if evolved purely as a non-singlet) and the WW function are employed (as is often done in the context of N^{k}LO+LL simulations), since they separately implement a unitary constraint; thus, an appropriate rescaling of the respective contributions must be envisaged.

Secondly, we note that in the context of an YFS-based approach all partonic processes that are not e^+e^--initiated enter (necessarily at orders at least one higher than the Born's) via the IR-finite residues. This implies that if photon-induced (or any other parton type) partonic processes give sizable contributions in a collinear-factorisation description owing predominantly to the all-order structure of the PDFs, such contributions cannot be reliably predicted by an YFS-based approach, unless the relevant collinear logarithms in the residues are resummed to all orders.

6.5 Simulations with beamstrahlung

In this section we consider the impact of beam-dynamics effects, which we identify with beamstrahlung, on the observable of eq. (6.4). Beamstrahlung is parametrised as indicated in eq. (2.1), so that the only initial-state particles we consider are electrons and positrons. As far as the function $\mathcal{B}_{e^+e^-}(y_+, y_-)$ is concerned, we use the form associated with a 500-GeV collider with an ILC-type configuration as is given in ref. [27]; the interested reader is urged to check that paper for further details. Here, we limit ourselves to pointing out that in our setup we define effective "beamstrahlung+ISR" PDFs, obtained by convoluting once and for all (i.e. prior to any physics runs) the beamstrahlung functions with the ISR PDFs, so that at runtime the number of integration variables is the same as that in the

JHEP10(2022)089

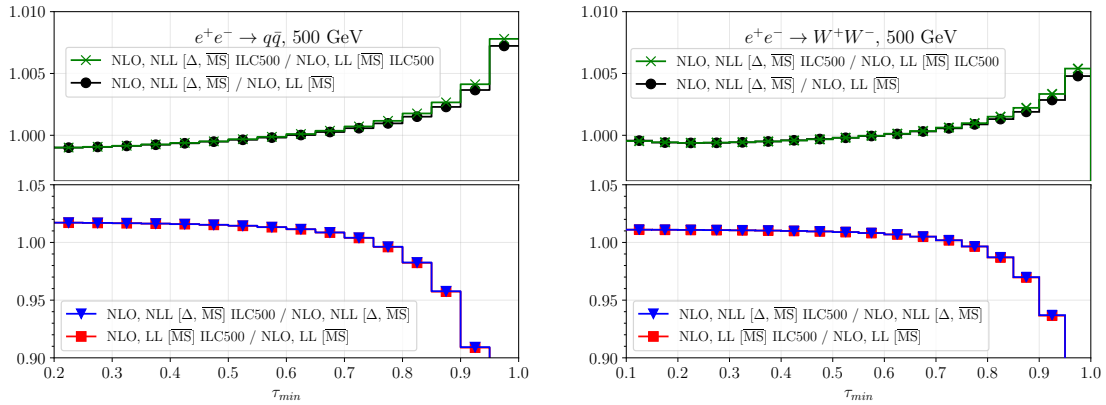

Figure 10. Results of simulations that include beamstrahlung effects at ILC500, and their comparisons with those obtained without beamstrahlung. See the text for details. Left panel: $q\bar{q}$ production; right panel: W^+W^- production.

case where beamstrahlung is ignored; this also implies that the numerical behaviour of the two environments is essentially identical.

Figure 10 presents the predictions for $q\bar{q}$ production (left panel) and W^+W^- production (right panel), whereas figure 11 is relevant to $t\bar{t}$ production, in the full SM (left panel) and in QED (right panel); the renormalisation scheme is chosen to be $\overline{\text{MS}}$, and NLO+NLL PDFs are defined in the Δ factorisation scheme. All panels have the same layout, namely: in the lower-half frame, we show the ratio of the cross section obtained by including beamstrahlung effects over that obtained by neglecting them, in the case of NLO+NLL PDFs (blue curves overlaid with triangles) and of LO+LL PDFs (red curves overlaid with boxes). In the upper-half frame, we show the ratio of the cross section obtained with NLO+NLL PDFs over that obtained with LO+LL PDFs, with (green curves overlaid with crosses) and without (black curves overlaid with circles) beamstrahlung effects — thus, the latter curves are exactly the same as those that appear in figures 2 and 3, and they are reported here for ease of comparison with their beamstrahlung-based counterparts. We can conclude what follows: for the configuration considered here (ILC-type), beamstrahlung effects have a clearly visible impact (up to $\mathcal{O}(10\%)$), which is observable-dependent and local. However, they affect in an almost identical manner the predictions stemming from LO+LL and NLO+NLL PDFs (the red and blue curves are very close to each other, and so are the black and green ones); this observation is valid for all of the production processes. The above implies that the conclusions drawn in sects. 6.2 and 6.3 apply to simulations with beamstrahlung as well.

7 Conclusions

This paper builds upon the results for the electron QED PDFs of refs. [22–24], and it features both theoretical and phenomenology material. From a theoretical viewpoint, the single-fermion-family UV-$\overline{\text{MS}}$ treatment of refs. [22–24] is extended to include the evolution

JHEP10(2022)089

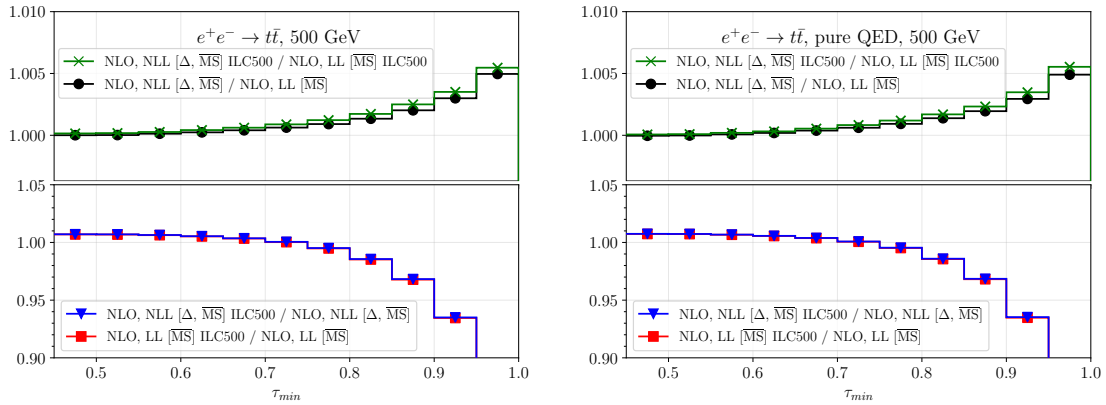

Figure 11. As in figure 10, for $t\bar{t}$ production in the full SM (left panel) and in QED (right panel).

with multiple fermion families and their mass thresholds, and to give one the possibility to choose among three different UV-renormalisation schemes ($\overline{\text{MS}}$, $\alpha(m_Z)$, and G_μ); for each of them, it is possible to adopt either the $\overline{\text{MS}}$ [23] or the Δ [24] factorisation scheme. From a phenomenology viewpoint, we have presented here for the first time in the literature fixed-order (LO and NLO) predictions for actual observables based on NLO+NLL PDFs. We have done so by exploiting the automated framework of MG5_aMC, thus improving the accuracy of the treatment of ISR in e^+e^- collisions w.r.t. that available in its previous public version [27], that was limited to LO+LL effects. An implication of this improvement is that now MG5_aMC can compute NLO EW corrections for processes with massless initial-state leptons, which was the only typology of NLO computations not publicly doable thus far. We also remark that the simulations of beamstrahlung effects introduced in ref. [27] remains viable in conjunction with NLO+NLL PDFs, and performs numerically as well as the LO+LL-based one.

The theoretical novelties presented here have different underlying motivations. The necessity of evolving PDFs with multiple fermion families stems from a requirement of consistency with the evolution of α which, if performed with a single fermion or without properly accounting for mass thresholds, would give a poor description of the data. Conversely, the possibility of choosing among different factorisation and renormalisation schemes gives one sufficient flexibility for high-energy simulations, regardless of whether a definite choice is made depending on the process and the running conditions under consideration, or whether theoretical systematics must be fully assessed. We note that which of these two options is adopted need not be the same for the factorisation and renormalisation schemes. In particular, we stress that for increasingly large energies the usage of fixed-α UV schemes such as $\alpha(m_Z)$ and G_μ may become questionable.

As far as phenomenology is concerned, our main conclusions are the following. At the level of observables, the NLL effects in the PDFs have an impact which is local (i.e. it depends on both the observable and its kinematical range), in both shape and size. It is thus impossible to account for it in a predictive and overall manner in the context of simulations based on LL-accurate PDFs. The differences between results obtained with different

JHEP10(2022)089

factorisation schemes at a given renormalisation scheme are generally much smaller than those between results obtained with different renormalisation schemes at a given factorisation scheme. For the inclusive observable we have studied here, the relative factorisation-scheme dependence is of $\mathcal{O}(10^{-4} - 10^{-3})$; should this figure, and its analogue for other observables, become comparable to or larger than the expected experimental accuracy, we note that there is some evidence that the Δ factorisation scheme is a better choice than $\overline{\text{MS}}$, since it has, w.r.t. the latter: a better behaviour in the soft region; a form closer in shape and size to the LL PDF (for the electron); and a better numerical stability in cross section computations. Finally, the approach we follow, based on collinear factorisation, renders it straightforward to include contributions due to partonic processes that are not e^+e^--initiated. As an example, we have considered the photon-induced contributions to W^+W^- and $t\bar{t}$ production, and found them to be very significant for the former process at small pair invariant masses. This is yet another example of an effect whose impact is local and process-dependent; it also shows why NLL-accurate evolution is to be preferred to an LL one, since it is only in the former case that electron PDFs associated with non-electron partons can unambiguously be defined.

The electron PDFs derived in this paper include all of the ingredients that are necessary for a systematic study of high-energy e^+e^- production processes which is both phenomenologically viable and of higher accuracy in its ISR treatment w.r.t. what has been done so far in the literature. Theoretically, the only item that remains to be addressed at the NLL is the possible inclusion of resummed soft non-collinear logarithms into the PDFs, which we leave to a future work. While this is conceptually interesting, we note that since the NLL PDFs defined here do exponentiate soft logarithms which are also collinear, when working at the NLO (or at the LO with the prescription introduced in appendix B) the effects not taken into account are at least of NNLO, and logarithmically subleading.

We finally remark that, together with this paper, we release both the code that returns the evolved electron PDFs (EMELA), and a new public version of MG5_AMC, that can be used to reproduce the results presented here.

Acknowledgments

SF is particularly indebted to G. Degrassi and A. Vogt for a few illuminating discussions. The help of D. de Florian, A. Denner, S. Forte, M. Greco, V. Hirschi, E. Laenen, D. Pagani, J. Reuter, H-S. Shao, and B. Ward at various stages of this work is also gratefully acknowledged. VB is supported by the European Union's Horizon 2020 research and innovation programme under grant agreement STRONG 2020 — No 824093. SF thanks the CERN TH Division for hospitality during the course of this work. MZ is supported by the "Programma per Giovani Ricercatori Rita Levi Montalcini" granted by the Italian Ministero dell'Università e della Ricerca (MUR). XZ is supported by the Italian Ministry of Research (MUR) under grant PRIN 20172LNEEZ. GS is supported in part by the Swiss National Science Foundation (SNF) under contract 200020-204200.

JHEP10(2022)089

A NLO cross sections with LO+LL PDFs

Let us suppose that the parton-level cross sections[31] $d\hat{\sigma}$ that enter eq. (1.2) are computed at $\mathcal{O}(\alpha^{b+p})$; with this, we understand that their Born contributions are of $\mathcal{O}(\alpha^b)$, and the overall perturbative accuracy is thus N^{p}LO. If the PDFs which such cross sections are convoluted with in eq. (1.2) are N^{q}LO accurate (the logarithmic accuracy is irrelevant in this argument, and is omitted), then the accuracy of the predicted particle-level cross sections $d\sigma$ is N$^{\min(p,q)}$LO, which follows trivially from a series expansion of the r.h.s. of eq. (1.2).

This is inconvenient, since typically $q < p$ — in particular, all of the phenomenological predictions published so far, with the exception of the NLO+NLL ones presented in this paper, have used LO-accurate PDFs (i.e. $q = 0$). This issue can be addressed by supplementing the partonic cross sections with a compensating contribution that features terms of $\mathcal{O}(\alpha^{q+1}, \dots \alpha^p)$, constructed (by using the perturbative expansion of the PDFs) so that the short-distance N^{p}LO accuracy is preserved by the convolution integral.

In this appendix we consider the case of NLO cross sections ($p = 1$) and LO PDFs ($q = 0$). We show that the compensating contribution can be written in a universal (i.e. process- and observable-independent) manner, and that it can be viewed (although improperly) as defining a PDF-specific factorisation scheme. In order to do that, we rewrite eq. (1.2) symbolically as follows:

$$d\sigma = \Gamma^{(K)} \star \Gamma^{(K)} \star d\hat{\sigma}^{(K)} \,, \tag{A.1}$$

where both the partonic cross sections and the PDFs are NLO-accurate for the time being. On the r.h.s. of eq. (A.1) we have included an upper index (K) to remind one explicitly that the corresponding quantities are factorisation-scheme dependent; order-by-order in perturbation theory, particle-level cross sections are factorisation-scheme independent, hence no index (K) appears on the l.h.s.. Using the conventions of eq. (3.41) for the perturbative coefficients of the series expansion of the PDFs, and their analogues for the cross sections, eq. (A.1) leads to:

$$d\sigma^{[0]} = d\hat{\sigma}^{[0]} \,, \tag{A.2}$$

$$d\sigma^{[1]} = d\hat{\sigma}^{(K)[1]} + d\delta^{(K)[1]} \,, \tag{A.3}$$

$$d\delta^{(K)[1]} = \Gamma^{(K)[1]} \star \Gamma^{[0]} \star d\hat{\sigma}^{[0]} + \Gamma^{[0]} \star \Gamma^{(K)[1]} \star d\hat{\sigma}^{[0]} \tag{A.4}$$

$$= \Gamma^{(K)[1]} \star d\hat{\sigma}^{[0]} + \Gamma^{(K)[1]} \star d\hat{\sigma}^{[0]} \,. \tag{A.5}$$

Equation (A.5) follows from eq. (A.4) because of eq. (3.42). Furthermore, $\Gamma^{(K)[1]}$ is given by the r.h.s. of eq. (3.43) (for the electron, which is the only relevant case since we shall eventually focus on LO PDFs) with $\mu_0 \to \mu$ there. By using the explicit formulae for the partonic cross sections of the FKS formalism [31, 32] one has:

$$d\hat{\sigma}^{(K)[1]} = d\hat{\sigma}^{(K=0)[1]} - d\kappa^{[1]} \,, \tag{A.6}$$

$$d\kappa^{[1]} = K \star d\hat{\sigma}^{[0]} + K \star d\hat{\sigma}^{[0]} \,. \tag{A.7}$$

[31] Particle and parton indices are understood throughout this appendix, in order to have a leaner notation; they play obvious roles, and the reader will have no difficulty in reinstating them if necessary.

JHEP10(2022)089

This shows that the l.h.s. of eq. (A.3) is indeed factorisation-scheme independent, since from eq. (3.43):

$$\Gamma^{(K)[1]} = \Gamma^{(K=0)[1]} + K\,. \tag{A.8}$$

We remind the reader that by setting $K = 0$ one works in the $\overline{\text{MS}}$ factorisation scheme.

If we now convolute the NLO partonic cross sections with LO PDFs Γ_{LO}, i.e. we write

$$d\sigma = \Gamma_{\text{LO}} \star \Gamma_{\text{LO}} \star d\hat{\sigma}^{(K)}\,, \tag{A.9}$$

instead of eq. (A.1), the analogues of eqs. (A.3) and (A.5) read:

$$d\sigma^{[1]} = d\hat{\sigma}^{(K)[1]} + d\delta^{[1]}_{\text{LO}}\,, \tag{A.10}$$

$$d\delta^{[1]}_{\text{LO}} = \Gamma^{[1]}_{\text{LO}} \star d\hat{\sigma}^{[0]} + \Gamma^{[1]}_{\text{LO}} \star d\hat{\sigma}^{[0]}\,, \tag{A.11}$$

respectively. It is clear that, in general, the l.h.s.'s of eqs. (A.3) and (A.10) are not equal to each other. However, one can *impose* them to be so, by equating their r.h.s.'s thus:

$$d\hat{\sigma}^{(K=0)[1]} + d\delta^{(K=0)[1]} = d\hat{\sigma}^{(K)[1]} + d\delta^{[1]}_{\text{LO}}\,, \tag{A.12}$$

where we have exploited the factorisation-scheme independence of eq. (A.3) to choose $K = 0$ there. Equation (A.12) is then solved for K (we denote the solution by K_{LO}), leading to:

$$K_{\text{LO}} = \Gamma^{[1]}_{\text{LO}} - \Gamma^{(K=0)[1]}\,. \tag{A.13}$$

When this function is used in eq. (A.7) (i.e. by setting $K = K_{\text{LO}}$ there), $d\kappa^{[1]}$ plays the role of the compensating contribution to the partonic cross sections (eq. (A.6)) which has been introduced in the discussion at the beginning of this appendix. We point out that the choice of the $\overline{\text{MS}}$ factorisation scheme in the second term on the r.h.s. of eq. (A.13) is dictated by simplicity. Still, another scheme could be chosen, but this would entail using it in the first term on the r.h.s. of eq. (A.6), since the property of scheme independence of the final result must be preserved.

Lest eq. (A.13) generate some misunderstanding, we stress that with LO PDFs the definition of a factorisation scheme does not make sense. However, the framework provided by the scheme-change functions K in the context of the FKS subtraction is very convenient for computing the compensating contribution that allows one to obtain NLO-accurate particle cross sections.

In order to be explicit, we now compute the K_{LO} functions for different LO PDFs. We write the generic functional form of the latter as follows:

$$\Gamma_{\text{LO}}(z) = \frac{\exp\left(3\beta_S/4 - \gamma_E\beta_E\right)}{\Gamma\left(1+\beta_E\right)}\,\beta_E(1-z)^{\beta_E-1} - \frac{1}{2}\beta_H(1+z) + \mathcal{O}(\alpha^2)\,. \tag{A.14}$$

We point out that both the $\mathcal{O}(\alpha^2)$ and $\mathcal{O}(\alpha^3)$ terms on the r.h.s. of eq. (A.14) are explicitly known [19–21, 23], but are not necessary to obtain the results that follow. Any choice of the parameters β_E, β_S, and β_H in eq. (A.14) is customarily (and unfortunately) called a "scheme"; here, we shall consider the following ones:

JHEP10(2022)089

- Beta scheme:
$$\beta_E = \beta_S = \beta_H = e_e^2 \beta \,. \tag{A.15}$$
- Eta scheme:
$$\beta_E = \beta_S = e_e^2 \beta \,, \qquad \beta_H = e_e^2 \eta \,. \tag{A.16}$$
- Mixed scheme:
$$\beta_E = e_e^2 \beta \,, \qquad \beta_S = \beta_H = e_e^2 \eta \,. \tag{A.17}$$
- Collinear scheme:
$$\beta_E = \beta_S = \beta_H = e_e^2 \eta_0 \,. \tag{A.18}$$
- Running scheme:
$$\beta_E = \beta_S = \beta_H = 2 e_e^2 t \,. \tag{A.19}$$

We have used the quantities:

$$\eta = \frac{\alpha}{\pi} \log \frac{\mu^2}{m^2} \,, \qquad \beta = \frac{\alpha}{\pi} \left(\log \frac{\mu^2}{m^2} - 1 \right) \,, \tag{A.20}$$

$$\eta_0 = \frac{\alpha}{\pi} \log \frac{\mu^2}{\mu_0^2} \,, \qquad t = \frac{1}{2\pi b_0} \log \frac{\alpha(\mu)}{\alpha(\mu_0)} = \frac{\alpha}{2\pi} \log \frac{\mu^2}{\mu_0^2} + \mathcal{O}(\alpha^2) \,. \tag{A.21}$$

The beta, eta, and mixed schemes are by now standard (see e.g. appendix A.1 of ref. [50]), while what we have called here collinear and running schemes are less so — we use them in the forms introduced in ref. [23], given there by eqs. (5.46) and (5.66), respectively, extended as is explained in sects. 3 and 4 to account for multiple fermion families and their thresholds (for previous single-fermion LL-accurate solutions with running α, see e.g. refs. [13, 16, 47]). Note that in the latter two schemes we have kept the dependence on the starting scale μ_0, rather than setting $\mu_0 = m$ as was done for the phenomenological applications of section 6. In a strict LO+LL evolution, the μ_0 dependence is beyond accuracy, but when convoluting with NLO cross sections some care is required, as we shall soon see.

We express the results for the $K_{\rm LO}$ functions in the various LO schemes considered in eqs. (A.15)–(A.19) by using the following functional form (which is the most general at this perturbative order):

$$K_{\rm LO}(z)/e_e^2 = K_\delta \delta(1-z) + K_+(z) \left(\frac{1}{1-z} \right)_+ + K_{\rm L}(z) \left(\frac{\log(1-z)}{1-z} \right)_+ + K_{reg}(z) \,. \tag{A.22}$$

The explicit computation of the r.h.s. of eq. (A.13) leads then to the following results:

- Beta scheme:
$$K_\delta = -\frac{7}{2} \,, \quad K_+(z) = 0 \,, \quad K_{\rm L}(z) = 2(1+z^2) \,, \quad K_{reg}(z) = 0 \,. \tag{A.23}$$
- Eta scheme:
$$K_\delta = -\frac{7}{2} \,, \quad K_+(z) = 0 \,, \quad K_{\rm L}(z) = 2(1+z^2) \,, \quad K_{reg}(z) = -(1+z) \,. \tag{A.24}$$

JHEP10(2022)089

- Mixed scheme:

$$K_\delta = -2\,, \quad K_+(z) = 0\,, \quad K_{\rm L}(z) = 2(1+z^2)\,, \quad K_{reg}(z) = -(1+z)\,. \tag{A.25}$$

- Collinear scheme:

$$K_\delta = -2 - \frac{3}{2}L_0\,, \quad K_+(z) = (1-L_0)(1+z^2)\,, \quad K_{\rm L}(z) = 2(1+z^2)\,, \quad K_{reg}(z) = 0\,. \tag{A.26}$$

- Running scheme:

$$\text{as in eq. (A.26)}\,. \tag{A.27}$$

Note that the results of eqs. (A.23)–(A.27) are specific to the $\overline{\rm MS}$ scheme (since eqs. (A.6) and (A.13) use $K = 0$), and must thus be used in conjunction not only with the appropriate LO+LL PDFs, but also with NLO short distance cross sections calculated in $\overline{\rm MS}$. Equivalent results appropriate for other factorisation schemes (i.e. with $K \neq 0$) can easily be derived.

In eq. (A.26) we have defined:

$$L_0 = \log\frac{\mu_0^2}{m^2}\,. \tag{A.28}$$

The dependence on μ_0 in the $K_{\rm LO}$ function defined by eq. (A.26) cancels at relative $\mathcal{O}(\alpha)$ against that of $\Gamma_{\rm LO}$ in the collinear and running schemes, so that the NLO particle cross section remains independent of μ_0, as is expected.

B LO cross sections with (N)LO+(N)LL PDFs

In appendix A we have shown how LO+LL PDFs must be used in conjunction with NLO short-distance cross sections without spoiling the accuracy of the latter. Here we consider the complementary question, namely: given LO-accurate cross sections (i.e. of $\mathcal{O}(\alpha^b)$), which PDFs should they be convoluted with (i.e. only LO+LL, or NLO+NLL as well)? We note that this is not an academic question: the vast majority of simulations relevant to BSM physics at future e^+e^- colliders still rely on LO cross sections.

From a formal viewpoint, at the level of observables the accuracy of predictions stemming from LO cross sections is LO, irrespective of whether LO+LL or NLO+NLL PDFs are used. However, numerically the choice of PDFs can have a much larger impact than simple perturbative considerations suggest. In order to see this, let us first make the obvious observation that in LO-based simulations all contributions factor out the $\mathcal{O}(\alpha^b)$ Born cross section.[32] In a proper NLO-accurate computation, contributions proportional to the Born emerge from three different sources:

a) the $\mathcal{O}(\alpha)$ term in the expansion of the PDFs;

[32]With some abuse of language, we shall say that such contributions are "proportional" to the Born, understanding a convolution.

JHEP10(2022)089

b) the degenerate $(n+1)$-body contributions to the short-distance cross sections;

c) the virtual, soft-, and collinear-reminder contributions to the short-distance cross sections.

We point out that, while items *b)* and *c)* are formulated in terms of quantities that appear in the FKS subtraction formalism, their analogues exist in any scheme that allows one to compute NLO results. Leaving aside the quantities in *c)* for the time being, and noting that we are only interested in the electron channel (since we shall eventually work at the LO), the kernel relevant to item *b)* can be read e.g. from eq. (4.88) of ref. [22], and re-written as follows:

$$\begin{aligned}\mathcal{K}_{ee}/e_e^2 = &\left[\frac{1+z^2}{1-z}\left(\log\frac{s}{\mu^2}+2\log(1-z)\right)\right]_+ + (1-z)\\ &+\left(\frac{7}{2}-\frac{3}{2}\log\frac{s}{\mu^2}\right)\delta(1-z) - K_{ee}(z)\,.\end{aligned} \tag{B.1}$$

Adding the r.h.s. of eq. (B.1) to the $\mathcal{O}(\alpha)$ term in the expansion of the PDFs (item *a)* above) leads to:

$$\begin{aligned}&\left(\Gamma_e^{(K)[1]}+\mathcal{K}_{ee}\right)/e_e^2 = \left(\Gamma_{\rm LO}^{[1]}+\mathcal{K}_{ee}\right)/e_e^2 =\\ &\quad\left(\frac{1+z^2}{1-z}\right)_+\left(\log\frac{s}{m^2}-1\right)+(1-z)+\left(\frac{7}{2}-\frac{3}{2}\log\frac{s}{\mu^2}\right)\delta(1-z)\,.\end{aligned} \tag{B.2}$$

A few comments on eq. (B.2) are in order. Firstly, as the notation suggests this result is relevant to both NLO+NLL PDFs and LO+LL PDFs. For this to happen, it is crucial that at the LO the $K_{\rm LO}$ functions derived in appendix A be used in $\mathcal{K}_{ee}$; conversely, with NLO+NLL PDFs the dependence on the K functions (i.e., on the factorisation scheme) disappears, as it should by construction. Secondly, at both the LO and the NLO the double-logarithmic term (present in both $\mathcal{K}_{ee}$ and the $\mathcal{O}(\alpha)$ term in the PDFs) also drops out; this is consistent with the usage of the PDFs in the factorisation theorem (eq. (1.2)), whose l.h.s. cannot have double-logarithmic terms of this kind given its nature of a massive-electron cross section. Thirdly, the term proportional to $\delta(1-z)$ has kinematically the same form as those from item *c)* above, and will naturally combine with them; in particular, this will imply the cancellation of the dependence upon μ.

We can now go back to the original problem posed in this appendix, namely that of the convolution of the PDFs with LO cross sections. In this case, only the contribution due to *a)* is relevant; with NLO+NLL PDFs, this implies a dependence of the result on the factorisation scheme (through the K functions) which, among other things, may induce an $\mathcal{O}(\alpha^{b+1})$ double-logarithmic term of the kind mentioned above (to be specific, this happens with $\overline{\rm MS}$ PDFs, but does *not* happen with those defined in the Δ scheme). Equation (B.2) then suggests a universal (i.e., process-independent) way to address this issue. The idea is the following: when performing an LO-based computation, one adds an $\mathcal{O}(\alpha^{b+1})$ term that has the same form as the degenerate $(n+1)$-body contribution; such a term is defined by

JHEP10(2022)089

means of the following kernel:

$$\mathcal{K}_{\mathrm{LO},ee}/e_e^2 = \left(\frac{1+z^2}{1-z}\right)_+ \log\frac{s}{\mu^2} + K_{ee}^{\mathrm{ref}}(z) - K_{ee}(z)\,. \tag{B.3}$$

Here, K_{ee}^{ref} is a scheme-change function associated with a fictitious "reference" scheme, that we determine as follows. Firstly, we require that when such a function is used in eq. (B.1) it cancels exactly all of the μ-independent terms for $z < 1$. This gives:

$$K_{ee}^{\mathrm{ref}}(z) = 2\,\frac{1+z^2}{1-z}\log(1-z) + (1-z)\,, \qquad z < 1\,. \tag{B.4}$$

Secondly, we extend the result of eq. (B.4) to all z's by adding an endpoint contribution proportional to $\delta(1-z)$, whose coefficient we compute by turning the functions in eq. (B.4) into plus distributions, and by requiring that the integral in $[0,1]$ of $K_{ee}^{\mathrm{ref}}(z)$ vanishes (this is equivalent to imposing a charge-conservation condition, see ref. [22]). Thus:

$$K_{ee}^{\mathrm{ref}}(z) = 2\left(\frac{1+z^2}{1-z}\log(1-z)\right)_+ + (1-z) - \frac{1}{2}\,\delta(1-z)\,. \tag{B.5}$$

Therefore, the inclusion of the term induced by the kernel of eq. (B.3) is so that at $\mathcal{O}(\alpha^{b+1})$ in an LO-based calculation one obtains a contribution:

$$\begin{aligned}\left(\Gamma_e^{(K)[1]} + \mathcal{K}_{\mathrm{LO},ee}\right)/e_e^2 &= \left(\Gamma_{\mathrm{LO}}^{[1]} + \mathcal{K}_{\mathrm{LO},ee}\right)/e_e^2 = \\ &\left(\frac{1+z^2}{1-z}\right)_+ \left(\log\frac{s}{m^2} - 1\right) + (1-z) - \frac{1}{2}\,\delta(1-z)\,.\end{aligned} \tag{B.6}$$

For comparison, e.g. in the Beta scheme one has:

$$\Gamma_{\mathrm{LO}}^{[1]}/e_e^2 = \left(\frac{1+z^2}{1-z}\right)_+ \left(\log\frac{\mu^2}{m^2} - 1\right). \tag{B.7}$$

Equation (B.6) shows that by following the procedure advocated here in the convolution of the LO cross sections with NLO+NLL PDFs there are no residual double-logarithmic terms at $\mathcal{O}(\alpha^{b+1})$, and no factorisation-scheme dependence. Conversely, when LO+LL PDFs are employed, the behaviour is quite analogous to that of a standard LO computation, with differences emerging solely from the inclusion of process-independent contributions (which also imply that the dependence upon the scale μ is of $\mathcal{O}(\alpha^{b+2})$ and not of $\mathcal{O}(\alpha^{b+1})$ as in eq. (B.7)[33]).

Clearly, there is ample freedom in the choice of the kernel of eq. (B.3). We stress again that the contribution it induces in the cross section is of $\mathcal{O}(\alpha^{b+1})$, and therefore

[33]This happens because the μ dependence of the non-$\delta(1-z)$ terms of eq. (B.3) is the same as that of eq. (B.1). As far as the $\delta(1-z)$ terms are concerned, it has already been observed that the μ dependence in eq. (B.1) is cancelled by that of the soft and collinear reminders. Although these are universal, for simplicity we have chosen to neglect them, and therefore we did not include a μ-dependent $\delta(1-z)$ term in eq. (B.3), bypassing the problem by imposing a charge-conservation condition.

JHEP10(2022)089

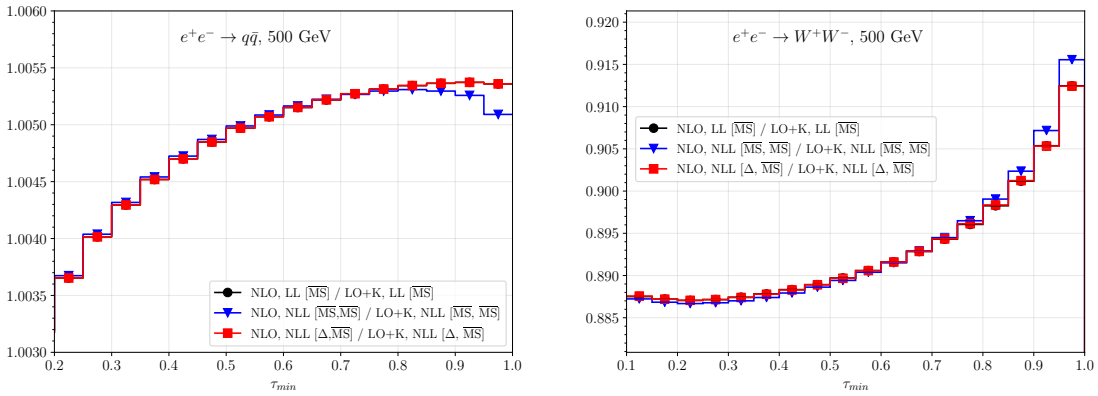

Figure 12. K-factors computed by including the contribution stemming from eq. (B.3) in the LO cross sections, in the $\overline{\text{MS}}$ renormalisation scheme for both NLL PDFs (in the $\overline{\text{MS}}$ and Δ factorisation schemes) and LL PDFs. Left panel: $q\bar{q}$ production; right panel: W^+W^- production.

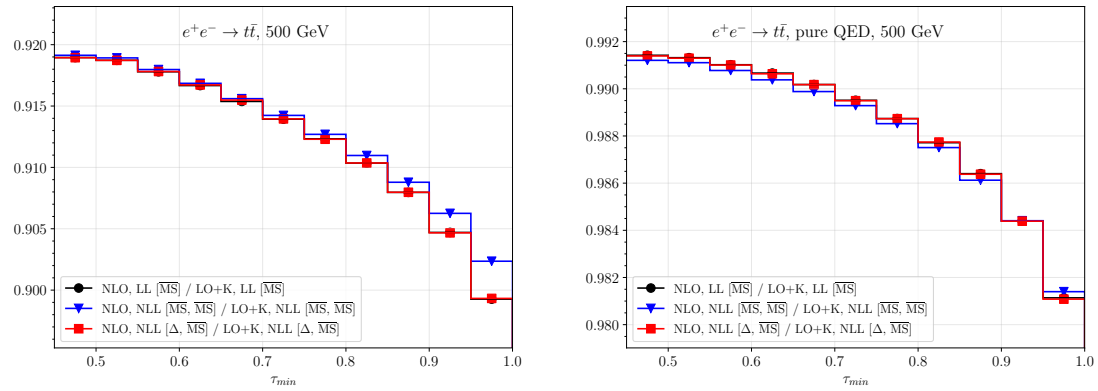

Figure 13. As in figure 12, for $t\bar{t}$ production in the full SM (left panel) and in QED (right panel).

formally beyond accuracy in the context of an LO-accurate computation. However, this procedure has at least a couple of positive features. Firstly, it prevents numerical results from becoming pathological, so that the coefficients of the perturbative expansion are well-behaved regardless of whether one employs LO+LL or NLO+NLL PDFs. And secondly, by making universal terms of $\mathcal{O}(\alpha^{b+1})$ independent of the PDF choice it emphasises the role of matrix elements (as opposed to PDFs) in the comparison between LO and NLO results. In other words, in this way one expects K-factors computed by including the convolution with PDFs to be quite similar to those obtained without such a convolution.

In order to see the impact of the procedure for the computation of LO-accurate cross sections discussed here, we present the results for the K-factors obtained by employing LO+LL (black curves overlaid with circles) and NLO+NLL PDFs (in the $\overline{\text{MS}}$ (blue curves overlaid with triangles) and Δ (red curves overlaid with boxes) schemes) *with* (figures 12 and 13) and *without* (figures 14 and 15) the inclusion of the contribution stemming from eq. (B.3). In order to be definite, we restrict ourselves to working with the $\overline{\text{MS}}$ renormalisation scheme.

JHEP10(2022)089

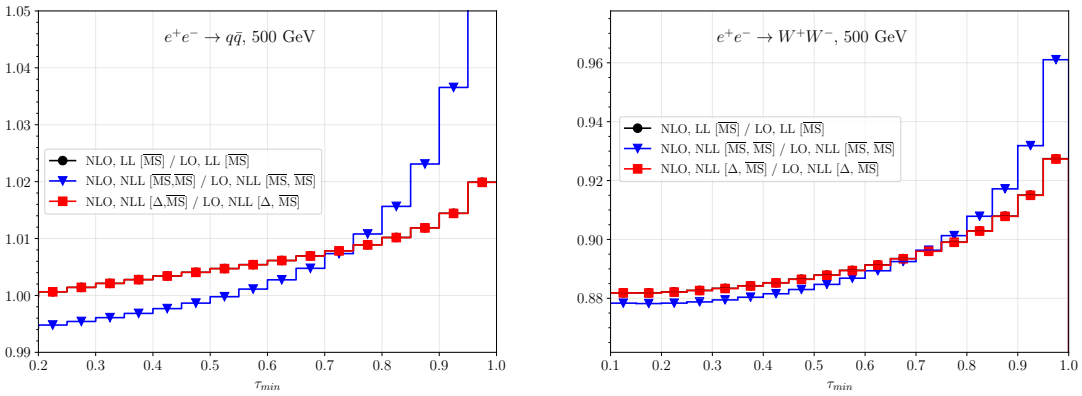

Figure 14. As in figure 12, with K-factors computed by *not* including the contribution stemming from eq. (B.3) in the LO cross sections. Left panel: $q\bar{q}$ production; right panel: W^+W^- production.

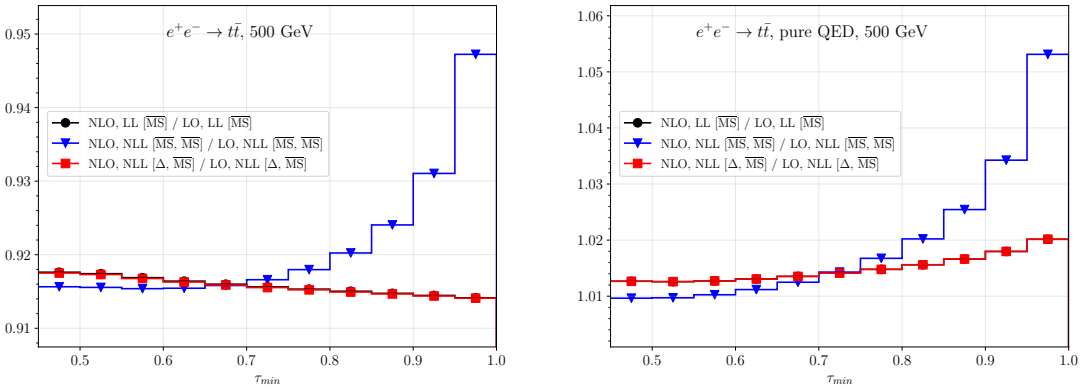

Figure 15. As in figure 14, for $t\bar{t}$ production in the full SM (left panel) and in QED (right panel).

Before proceeding to commenting the results, we make two observations. Firstly, significant differences between K-factors computed with different prescriptions and/or choices of factorisation scheme are predominantly induced by the denominators (i.e. by the LO cross sections), since we have seen in sects. 6.2 and 6.3 that NLO results are all relatively close to each other under the same conditions. Secondly, regardless of their definitions K-factors remain unphysical quantities, that cannot be used to draw conclusions about physics issues.

The main implication of figures 12–15 is that by using eq. (B.3) the K-factors computed with the three different PDF choices are close to each other, while with the standard definition those obtained by using NLO+NLL $\overline{\text{MS}}$-defined PDFs are clear outliers. The analytical formulae presented above show that this is due to the presence, in the LO-accurate results computed in the standard manner with such PDFs, of double-logarithmic terms that must not feature at observable level on the l.h.s. of the factorisation formula, and do so on the r.h.s. owing only to their being beyond accuracy. Conversely, and regardless of the specific definition adopted for the K-factor, results obtained with LO+LL PDFs are quite similar to those obtained with NLO+NLL Δ-defined PDFs (in fact, with the y ranges used in the plots, they are essentially indistinguishable from one another). This is

JHEP10(2022)089

consistent with the observation already made about figure 4, that the electron densities stemming from these two PDFs are quite similar in shape and size.

We can further observe that, in the case of LO+LL PDFs and NLO+NLL ones with the Δ factorisation scheme, K-factors computed with eq. (B.3) or without it are close to each other, with the quality of such an agreement decreasing with $\tau_{\rm min}$. This is not surprising, in view of the fact that K-factors are meant to quantify inclusive properties, and the level of inclusiveness decreases with $\tau_{\rm min}$ (to the extent that at $\tau_{\rm min} \simeq 1$ one exposes the presence of soft logarithms). Furthermore, the K-factors relevant to the processes computed in QED are closer to one than their full-SM counterparts — this is the origin of the behaviour underlined in section 6.3, namely that the former processes have a smaller factorisation-scheme dependence w.r.t. the latter ones.

C NLO EW corrections with massless initial-state leptons

In this appendix, we document the changes to the MG5_aMC code that have occurred for the computation of NLO EW corrections at lepton colliders to become possible. We remind the reader that MG5_aMC has originally automated NLO QCD corrections [25]; this has later been extended [26] to the case of NLO EW (and mixed, i.e. the simultaneous perturbative expansion in two coupling constants) corrections. Technically, the NLO implementations of refs. [25, 26] are based on the assumption that the initial-state partons that initiate the hard process are not monochromatic, but rather have non-trivial energy spectra, which are given by the PDFs. In view of the fact that the emphasis of refs. [25, 26] is hadronic physics, such PDFs has been taken so far to be the hadronic ones. Thus, in order to extend the NLO-EW-correction capabilities of MG5_aMC to e^+e^- collisions, a precondition is the implementation of electron PDFs, which pose a challenging numerical problem in view of their integrable-singularity behaviour at $z \to 1$. This issue has been addressed in ref. [27], whose solution is however limited to cross sections which are LO-accurate in α.

In summary: given what has been achieved for EW corrections in ref. [26] (complete automation of NLO matrix elements, and of NLO cross sections in hadronic collisions) and ref. [27] (inclusion in MG5_aMC of electron PDFs), in the present work we have addressed the only remaining missing item, namely the automation of the computations of NLO-EW cross sections in the presence of electron PDFs. Here, the key issue (which sets this case apart from its LO-EW counterpart solved in ref. [27]) is the efficiency of the phase-space integration of locally-subtracted real-emission matrix elements, which is severely degraded in the presence of electron PDFs, and specifically because of that of the electron/positron (i.e. $\Gamma_{e^\pm/e^\pm}$).

The nature of the problem is the following: in MG5_aMC the cancellation of soft and collinear divergences relies on the FKS subtraction formalism [31, 32] and on its automation (see ref. [33]). FKS first achieves a simplification of the singularity structure of the matrix elements by effectively partitioning the phase space into sectors, identified by two parton indices i (the FKS parton) and j (its sister), so that in each of them at most one soft (when $E_i \to 0$) and one collinear (when $\theta_{ij} \to 0$) singularity occurs. If parton j belongs to the

JHEP10(2022)089

initial state, the way in which the real-emission kinematics is generated in MG5_aMC is based on the so-called event projection (see e.g. refs. [17, 51]): the sum of all final-state momenta bar that of parton i has the same invariant mass and rapidity as the sum of the final-state momenta in the underlying Born kinematics. This procedure, that requires initial-state partons to be non-monochromatic, is a necessary feature in order to be able to match NLO computations with current *hadronic* parton showers, as it mimics what the latter do in the case of initial-state backward evolution. It is not mandatory, but greatly improves the integration efficiency, in the case of fixed-order computations. One of the implications of event projection is that it leads to the fact that real-emission matrix elements and their subtraction terms are associated with different Bjorken x's. While this is not a problem in the case of hadronic collisions (since the PDFs are slowly decreasing functions), in the case of e^+e^- collisions (with the PDFs sharply increasing functions) it creates serious efficiency issues.

In order to cope with this problem, in MG5_aMC a new way of generating the real-emission kinematics has been introduced, and applied to those FKS sectors relevant to the cases where the (massless) FKS sister j is in the initial state and the underlying branching is a QED one. More in detail, we proceed as was anticipated in section 6 of ref. [42], namely:

1. The four-momentum k_i of the FKS parton i is generated by means of the variables:

$$\xi_i = \frac{2E_i}{\sqrt{\hat{s}}}\,, \quad y_{ij} = \cos\theta_{ij}\,, \quad \varphi_{ij}\,. \tag{C.1}$$

   These correspond to the rescaled (w.r.t. the c.m. partonic energy $\sqrt{\hat{s}}$) energy of the FKS parton, its polar angle w.r.t. the FKS sister j, and an azimuthal angle φ_{ij}, respectively, all of which are defined in the partonic c.m. frame. These variables are in a one-to-one correspondence with some integration random numbers (generally with adaptive sampling).

2. The kinematics of the other n final-state momenta $\{\bar{k}_l\}_{l=1,n+1}^{l\neq i}$ is first generated in their c.m. frame, knowing that their total invariant mass squared is:

$$\left(\sum_{\substack{l=1\\l\neq i}}^{n+1}\bar{k}_l\right)^2 = (1-\xi_i)\,\hat{s}\,. \tag{C.2}$$

3. Finally, the momenta $\{\bar{k}_l\}_{l=1,n+1}^{l\neq i}$ are boosted in the partonic c.m. frame

$$k_l = \mathbf{B}\bar{k}_l \tag{C.3}$$

   with the boost $\mathbf{B}$ along the three-direction of k_i, and so that total momentum conservation is achieved, namely:

$$\sum_{l=1}^{n+1} k_l = \left(\sqrt{\hat{s}},\vec{0}\right)\,. \tag{C.4}$$

JHEP10(2022)089

In this way, a stable and efficient evaluation of NLO EW corrections can be performed also for lepton collisions within MG5_aMC.

We point out that, since the generation of momenta outlined above does not rely on event projection, it is also incompatible with an MC@NLO-type matching for initial-state QED emissions, *assuming* that for these kinds of branchings Parton Shower Monte Carlos work precisely in the same way as they do in hadronic collisions. This assumption is not necessarily correct, but is in any case useful to remind one that an NLO-accurate matrix element-Monte Carlo matching for e^+e^- collisions constitutes an open problem, whose solution is highly desirable.

D Synopsis of previous results on NLO+NLL PDFs

In view of the systematic usage of the results of refs. [22–24] made in this paper, we give here some additional information about them, which complement the discussion in section 2. While this renders the current work essentially self-contained, for a fuller understanding of the issues involved the reader is urged to consult the original publications.

We start by pointing out again that refs. [22–24] are based on considering a single lepton family and on working in the $\overline{\text{MS}}$ renormalisation scheme; both of these limitations have been lifted in this paper. Then:

- In ref. [22] the NLO (i.e. $\mathcal{O}(\alpha)$) initial conditions are computed, for both PDFs and fragmentation functions (FFs) and for any combination of particle (i.e. the object that branches) and parton (i.e. the object that emerges from the branching and enters the short-distance cross section).[34] Such NLO initial conditions are factorisation-scale dependent, and are meant to be imposed at a scale $\mu = \mu_0 \sim m$ in order to start the evolution. Furthermore, at any generic value of μ they coincide by construction with the $\mathcal{O}(\alpha)$ expansions of the respective PDFs and FFs. In the case of the PDFs, they are reported here in eqs. (3.42)–(3.45).

- In ref. [23] the NLO initial conditions computed in ref. [22] are employed to obtain the NLL-evolved PDFs for an electron particle (in other words, PDFs for a photon particle and FFs are not considered, but can be dealt with in a pretty analogous manner). Ref. [23] works in the $\overline{\text{MS}}$ factorisation scheme, and achieves the sought-for NLL-evolved PDFs in three different ways: *a)* analytically to all orders in α for $z \to 1$ (this is called the asymptotic solution); *b)* analytically up to $\mathcal{O}(\alpha^3)$ for $z < 1$ (this is called the recursive solution); *c)* numerically for any $z \lesssim 1 - 10^{-\kappa}$, with $\kappa \simeq 10$ (this is called the numerical solution). The asymptotic and recursive solutions are then matched to each other additively, and found to agree extremely well with the numerical solution for all of the z values where the latter is reliable. While this provides one with a powerful self-consistency check, in practical applications it is more convenient to employ the numerical solution for $z \lesssim 1$, and to switch to the asymptotic one when $z \to 1$. The availability of the latter in an analytic form is

[34] This applies to spacelike branchings (i.e. to PDFs); the role of particle and parton is reversed in timelike branchings (i.e. for FFs).

JHEP10(2022)089

crucial in particular for the electron parton, in view of the fact that its PDFs has a power-like integrable divergence at $z = 1$.

- In ref. [24] the NLO initial conditions computed in ref. [22] are employed to obtain the NLL-evolved PDFs for an electron particle by working in a DIS-inspired factorisation scheme, called Δ, expected to be better behaved in the $z \sim 1$ region w.r.t. the $\overline{\text{MS}}$ factorisation scheme. Given the final remark of the previous bullet point, at variance with ref. [23] only the asymptotic solution has been considered. More in detail, two different solutions, called Δ_1 and Δ_2, have been obtained in ref. [24], which differ from each other in the fact that certain effects in the running of α are kept to all orders in the former, while are limited to $\mathcal{O}(\alpha^2)$ in the latter. As it turns out, the Δ_1 solution is vastly superior. Therefore, the Δ_2 one has not been considered any further, and in order to simplify the notation the Δ-scheme results of this paper coincide with those stemming from the Δ_1 solution of ref. [24].

As it has been pointed out in sects. 3 and 4, the functional forms of the asymptotic solutions of refs. [23, 24] are unchanged in the case of an evolution with multiple fermion families,[35] and only the parametric replacements of eq. (3.67) are necessary (plus $t \to t_k$ in the case of the photon PDFs). For the reader's convenience, we report below such functional forms, which are implicitly employed in sects. 3 and 4 of this paper.

- Electron parton, $\overline{\text{MS}}$ factorisation scheme. This is eq. (5.63) of ref. [23]:

$$\Gamma_{e^-}^{(\overline{\text{MS}})}(z,\mu) \overset{z\to 1}{\longrightarrow} \frac{e^{-\gamma_{\text{E}}\xi_1} e^{\hat{\xi}_1}}{\Gamma(1+\xi_1)}\,\xi_1(1-z)^{-1+\xi_1} \times \left\{1 + \frac{\alpha(\mu_0)}{\pi}\left[\left(\log\frac{\mu_0^2}{m^2} - 1\right)\left(A(\xi_1) + \frac{3}{4}\right) - 2B(\xi_1) + \frac{7}{4} + \left(\log\frac{\mu_0^2}{m^2} - 1 - 2A(\xi_1)\right)\log(1-z) - \log^2(1-z)\right]\right\}. \tag{D.1}$$

- Photon parton, $\overline{\text{MS}}$ factorisation scheme. This is eq. (B.87)[36] of ref. [23]:

$$\Gamma_{\gamma}^{(\overline{\text{MS}})}(z,\mu) \overset{z\to 1}{\longrightarrow} \frac{t\,\alpha(\mu_0)^2}{\alpha(\mu)}\,\frac{3}{2\pi\xi_1}\,\log(1-z) - \frac{t\,\alpha(\mu_0)^3}{\alpha(\mu)}\,\frac{1}{2\pi^2\xi_1}\,\log^3(1-z)\,. \tag{D.2}$$

- Electron parton, Δ factorisation scheme. This is eq. (4.40) of ref. [24]:

$$\Gamma_{e^-}^{(\Delta)}(z,\mu) \overset{z\to 1}{\longrightarrow} \frac{e^{-\gamma_{\text{E}}\xi_1} e^{\hat{\xi}_1}}{\Gamma(1+\xi_1)}\,\xi_1(1-z)^{-1+\xi_1} \times \left[\left(1 + \frac{3\alpha(\mu_0)}{4\pi}L_0\right)\sum_{p=0}^{\infty}\mathcal{S}_{1,p}(z) - \frac{\alpha(\mu_0)}{\pi}L_0\sum_{p=0}^{\infty}\mathcal{S}_{2,p}(z)\right]. \tag{D.3}$$

[35] Note that PDFs for partons different from the electron and the photon vanish for $z \to 1$.

[36] Where use is made of eq. (B.25) of ref. [23] to obtain a numerically-equivalent form which is more convenient in practical applications.

JHEP10(2022)089

- Photon parton, Δ factorisation scheme. This is eq. (5.50) of ref. [24]:

$$\Gamma_\gamma^{(\Delta)}(z,\mu) \overset{z\to 1}{\longrightarrow} \frac{1}{2\pi}\,\frac{\alpha^2(\mu_0)}{\alpha(\mu)}\,\frac{1+(1-z)^2}{z}\,L_0 + \frac{1}{2\pi\xi_1}\,\frac{t\,\alpha^2(\mu_0)}{\alpha(\mu)}\,L_0 - \frac{t\,\alpha(\mu)}{2\pi\xi_1}\,\frac{e^{-\gamma_{\rm E}\xi_1}e^{\hat{\xi}_1}}{\Gamma\,(1+\xi_1)}\,(1-z)^{\xi_1}\,L_0\,. \tag{D.4}$$

In these equations, several secondary quantities are employed. L_0 has been defined in eq. (A.28). We also have the identities:

$$d_1(\xi) \,=\, -A(\xi)\,, \tag{D.5}$$

$$d_2(\xi) \,=\, 2B(\xi) - \frac{\pi^2}{6}\,, \tag{D.6}$$

with:

$$d_k(\xi) \,=\, \frac{1}{\mathcal{G}_d(\xi,0)}\,\frac{\partial^k \mathcal{G}_d(\xi,\delta)}{\partial\delta^k}\bigg|_{\delta=0}\,, \tag{D.7}$$

$$\mathcal{G}_d(\xi,\delta) \,=\, \frac{e^{-\gamma_{\rm E}(\xi-\delta)}}{\Gamma(\xi-\delta)}\,. \tag{D.8}$$

The functions $\mathcal{S}_{i,p}(z)$ that appear on the r.h.s. of eq. (D.3) are:

$$\mathcal{S}_{1,p}(z) \,=\, \delta_{p0}\,\frac{\alpha(\mu)}{\alpha(\mu_0)} + \frac{\alpha(\mu)-\alpha(\mu_0)}{\pi}\,\frac{\hat{\mathcal{S}}_{1,p}(z)}{D(z)^{p+1}}\,, \tag{D.9}$$

$$\mathcal{S}_{2,p}(z) \,=\, \frac{\alpha(\mu)}{\alpha(\mu_0)}\Big(-\delta_{p0}\log(1-z) + \delta_{p1}d_1(\xi_1)\Big) + \frac{\alpha(\mu)-\alpha(\mu_0)}{\pi}\,\frac{\hat{\mathcal{S}}_{2,p}(z)}{D(z)^{p+1}}\,, \tag{D.10}$$

and have the following properties:

$$\frac{\hat{\mathcal{S}}_{1,p}(z)}{D(z)^{p+1}} \overset{z\to 1}{\longrightarrow} \log^{-2-p}(1-z) \;\longrightarrow\; 0\,, \tag{D.11}$$

$$\frac{\hat{\mathcal{S}}_{2,p}(z)}{D(z)^{p+1}} \overset{z\to 1}{\longrightarrow} \log^{-1-p}(1-z) \;\longrightarrow\; 0\,, \tag{D.12}$$

where

$$D(z) = 1 + \frac{\alpha(\mu_0)}{\pi}\,\log^2(1-z)\,. \tag{D.13}$$

The functions above can be computed recursively for any p, starting from their definitions given in eqs. (4.18), (4.29), and (4.30) of ref. [24], but owing to eqs. (D.11) and (D.12) only

JHEP10(2022)089

the lowest p values are needed in numerical computations. From ref. [24]:

$$\hat{\mathcal{S}}_{1,0}(z) = -\frac{\pi}{\alpha(\mu_0)}\,, \tag{D.14}$$

$$\hat{\mathcal{S}}_{1,1}(z) = (1 - 2d_1(\xi_1))\log(1-z)\,, \tag{D.15}$$

$$\begin{aligned}\hat{\mathcal{S}}_{1,2}(z) = {} & \frac{\alpha(\mu_0)}{\pi}\left(C - 1 + 3d_1(\xi_1) - 3d_2(\xi_1)\right)\log^2(1-z) \\ & + C - d_1(\xi_1) + d_2(\xi_1)\,,\end{aligned} \tag{D.16}$$

$$\hat{\mathcal{S}}_{2,0}(z) = \frac{\pi}{\alpha(\mu_0)}\log(1-z)\,, \tag{D.17}$$

$$\hat{\mathcal{S}}_{2,1}(z) = -(1 - d_1(\xi_1))\log^2(1-z) - \frac{\pi}{\alpha(\mu_0)}\,d_1(\xi_1)\,, \tag{D.18}$$

$$\begin{aligned}\hat{\mathcal{S}}_{2,2}(z) = {} & -\frac{\alpha(\mu_0)}{\pi}\left(C - 1 + 2d_1(\xi_1) - d_2(\xi_1)\right)\log^3(1-z) \\ & - \Big(C - 2d_1(\xi_1) + 3d_2(\xi_1)\Big)\log(1-z)\,,\end{aligned} \tag{D.19}$$

and:

$$C = \frac{\pi^2}{6} - 1\,. \tag{D.20}$$

In the numerical implementation these contributions have actually been included up to $p = 5$; we refrain from reporting here the corresponding analytical expressions, which are cumbersome without being particularly illuminating.

References

[1] CEPC Study Group collaboration, *CEPC Conceptual Design Report: Volume 2 - Physics & Detector*, arXiv:1811.10545 [INSPIRE].

[2] FCC collaboration, *FCC-ee: The Lepton Collider*: Future Circular Collider Conceptual Design Report Volume 2, *Eur. Phys. J. ST* **228** (2019) 261 [INSPIRE].

[3] P. Bambade et al., *The International Linear Collider: A Global Project*, arXiv:1903.01629 [INSPIRE].

[4] CLICdp, CLIC collaboration, *The Compact Linear Collider (CLIC) - 2018 Summary Report*, arXiv:1812.06018 [INSPIRE].

[5] E.A. Kuraev and V.S. Fadin, *On Radiative Corrections to e^+e^- Single Photon Annihilation at High-Energy*, *Sov. J. Nucl. Phys.* **41** (1985) 466 [INSPIRE].

[6] J.R. Ellis and R. Peccei, *Physics at lep. 1.*, CERN-86-02-V-1 [INSPIRE].

[7] D.R. Yennie, S.C. Frautschi and H. Suura, *The infrared divergence phenomena and high-energy processes*, *Annals Phys.* **13** (1961) 379 [INSPIRE].

[8] S. Jadach, B.F.L. Ward and Z. Was, *Coherent exclusive exponentiation for precision Monte Carlo calculations*, *Phys. Rev. D* **63** (2001) 113009 [hep-ph/0006359] [INSPIRE].

JHEP10(2022)089

[9] H. Anlauf, H.D. Dahmen, P. Manakos, T. Mannel and T. Ohl, *KRONOS: A Monte Carlo event generator for higher order electromagnetic radiative corrections to deep inelastic scattering at HERA*, *Comput. Phys. Commun.* **70** (1992) 97 [INSPIRE].

[10] J. Fujimoto, Y. Shimizu and T. Munehisa, *Monte Carlo approach to radiative processes in e^+e^- annihilation*, *Prog. Theor. Phys.* **90** (1993) 177 [INSPIRE].

[11] T. Munehisa, J. Fujimoto, Y. Kurihara and Y. Shimizu, *Improved QEDPS for radiative corrections in e^+e^- annihilation*, *Prog. Theor. Phys.* **95** (1996) 375 [hep-ph/9603322] [INSPIRE].

[12] C.M. Carloni Calame, C. Lunardini, G. Montagna, O. Nicrosini and F. Piccinini, *Large angle Bhabha scattering and luminosity at flavor factories*, *Nucl. Phys. B* **584** (2000) 459 [hep-ph/0003268] [INSPIRE].

[13] V.N. Gribov and L.N. Lipatov, *Deep inelastic e p scattering in perturbation theory*, *Sov. J. Nucl. Phys.* **15** (1972) 438 [INSPIRE].

[14] L.N. Lipatov, *The parton model and perturbation theory*, *Sov. J. Nucl. Phys.* **20** (1975) 94.

[15] G. Altarelli and G. Parisi, *Asymptotic Freedom in Parton Language*, *Nucl. Phys. B* **126** (1977) 298 [INSPIRE].

[16] Y.L. Dokshitzer, *Calculation of the Structure Functions for Deep Inelastic Scattering and e^+e^- Annihilation by Perturbation Theory in Quantum Chromodynamics*, *Sov. Phys. JETP* **46** (1977) 641 [INSPIRE].

[17] S. Frixione and B.R. Webber, *Matching NLO QCD computations and parton shower simulations*, *JHEP* **06** (2002) 029 [hep-ph/0204244] [INSPIRE].

[18] P. Nason, *A New method for combining NLO QCD with shower Monte Carlo algorithms*, *JHEP* **11** (2004) 040 [hep-ph/0409146] [INSPIRE].

[19] M. Skrzypek and S. Jadach, *Exact and approximate solutions for the electron nonsinglet structure function in QED*, *Z. Phys. C* **49** (1991) 577 [INSPIRE].

[20] M. Skrzypek, *Leading logarithmic calculations of QED corrections at LEP*, *Acta Phys. Polon. B* **23** (1992) 135 [INSPIRE].

[21] M. Cacciari, A. Deandrea, G. Montagna and O. Nicrosini, *QED structure functions: A Systematic approach*, *EPL* **17** (1992) 123 [INSPIRE].

[22] S. Frixione, *Initial conditions for electron and photon structure and fragmentation functions*, *JHEP* **11** (2019) 158 [arXiv:1909.03886] [INSPIRE].

[23] V. Bertone, M. Cacciari, S. Frixione and G. Stagnitto, *The partonic structure of the electron at the next-to-leading logarithmic accuracy in QED*, *JHEP* **03** (2020) 135 [*Erratum ibid.* **08** (2022) 108] [arXiv:1911.12040] [INSPIRE].

[24] S. Frixione, *On factorisation schemes for the electron parton distribution functions in QED*, *JHEP* **07** (2021) 180 [*Erratum ibid.* **12** (2012) 196] [arXiv:2105.06688] [INSPIRE].

[25] J. Alwall et al., *The automated computation of tree-level and next-to-leading order differential cross sections, and their matching to parton shower simulations*, *JHEP* **07** (2014) 079 [arXiv:1405.0301] [INSPIRE].

[26] R. Frederix, S. Frixione, V. Hirschi, D. Pagani, H.S. Shao and M. Zaro, *The automation of next-to-leading order electroweak calculations*, *JHEP* **07** (2018) 185 [*Erratum ibid.* **11** (2021) 085] [arXiv:1804.10017] [INSPIRE].

JHEP10(2022)089

[27] S. Frixione, O. Mattelaer, M. Zaro and X. Zhao, *Lepton collisions in MadGraph5_aMC@NLO*, arXiv:2108.10261 [INSPIRE].

[28] S. Dittmaier and M. Krämer, *Electroweak radiative corrections to W boson production at hadron colliders*, *Phys. Rev. D* **65** (2002) 073007 [hep-ph/0109062] [INSPIRE].

[29] A. Denner, *Techniques for calculation of electroweak radiative corrections at the one loop level and results for W physics at LEP-200*, *Fortsch. Phys.* **41** (1993) 307 [arXiv:0709.1075] [INSPIRE].

[30] D. de Florian, G.F.R. Sborlini and G. Rodrigo, *Two-loop QED corrections to the Altarelli-Parisi splitting functions*, *JHEP* **10** (2016) 056 [arXiv:1606.02887] [INSPIRE].

[31] S. Frixione, Z. Kunszt and A. Signer, *Three jet cross-sections to next-to-leading order*, *Nucl. Phys. B* **467** (1996) 399 [hep-ph/9512328] [INSPIRE].

[32] S. Frixione, *A General approach to jet cross-sections in QCD*, *Nucl. Phys. B* **507** (1997) 295 [hep-ph/9706545] [INSPIRE].

[33] R. Frederix, S. Frixione, F. Maltoni and T. Stelzer, *Automation of next-to-leading order computations in QCD: The FKS subtraction*, *JHEP* **10** (2009) 003 [arXiv:0908.4272] [INSPIRE].

[34] Particle Data Group collaboration, *Review of Particle Physics*, *PTEP* **2020** (2020) 083C01 [INSPIRE].

[35] G. Degrassi and A. Vicini, *Two loop renormalization of the electric charge in the standard model*, *Phys. Rev. D* **69** (2004) 073007 [hep-ph/0307122] [INSPIRE].

[36] J.C. Collins, F. Wilczek and A. Zee, *Low-Energy Manifestations of Heavy Particles: Application to the Neutral Current*, *Phys. Rev. D* **18** (1978) 242 [INSPIRE].

[37] V. Bertone, S. Carrazza, D. Pagani and M. Zaro, *On the Impact of Lepton PDFs*, *JHEP* **11** (2015) 194 [arXiv:1508.07002] [INSPIRE].

[38] V. Bertone, S. Carrazza and E.R. Nocera, *Reference results for time-like evolution up to* $\mathcal{O}\left(\alpha_s^3\right)$, *JHEP* **03** (2015) 046 [arXiv:1501.00494] [INSPIRE].

[39] M. Bonvini, *Resummation of soft and hard gluon radiation in perturbative QCD*, PhD thesis, Genoa University (2012), arXiv:1212.0480 [INSPIRE].

[40] W. Magnus, *On the exponential solution of differential equations for a linear operator*, *Commun. Pure Appl. Math.* **7** (1954) 649.

[41] NNPDF collaboration, L. Del Debbio, S. Forte, J.I. Latorre, A. Piccione and J. Rojo, *Neural network determination of parton distributions: The Nonsinglet case*, *JHEP* **03** (2007) 039 [hep-ph/0701127] [INSPIRE].

[42] S. Frixione et al., *Initial state QED radiation aspects for future* e^+e^- *colliders*, in *2022 Snowmass Summer Study*, (2022), arXiv:2203.12557 [INSPIRE].

[43] A. Buckley et al., *LHAPDF6: parton density access in the LHC precision era*, *Eur. Phys. J. C* **75** (2015) 132 [arXiv:1412.7420] [INSPIRE].

[44] C.W. Bauer, N. Ferland and B.R. Webber, *Standard Model Parton Distributions at Very High Energies*, *JHEP* **08** (2017) 036 [arXiv:1703.08562] [INSPIRE].

[45] B. Fornal, A.V. Manohar and W.J. Waalewijn, *Electroweak Gauge Boson Parton Distribution Functions*, *JHEP* **05** (2018) 106 [arXiv:1803.06347] [INSPIRE].

JHEP10(2022)089

[46] C.W. Bauer and B.R. Webber, *Polarization Effects in Standard Model Parton Distributions at Very High Energies*, *JHEP* **03** (2019) 013 [arXiv:1808.08831] [INSPIRE].

[47] O. Nicrosini and L. Trentadue, *Soft Photons and Second Order Radiative Corrections to* $e^+e^- \to Z0$, *Phys. Lett. B* **196** (1987) 551 [INSPIRE].

[48] C.F. von Weizsacker, *Radiation emitted in collisions of very fast electrons*, *Z. Phys.* **88** (1934) 612 [INSPIRE].

[49] E.J. Williams, *Nature of the high-energy particles of penetrating radiation and status of ionization and radiation formulae*, *Phys. Rev.* **45** (1934) 729 [INSPIRE].

[50] W. Beenakker et al., *WW cross-sections and distributions*, in *CERN Workshop on LEP2 Physics (followed by 2nd meeting, 15-16 Jun 1995 and 3rd meeting 2-3 Nov 1995)*, 2, 1996. hep-ph/9602351 [INSPIRE].

[51] R. Frederix, S. Frixione, V. Hirschi, F. Maltoni, R. Pittau and P. Torrielli, *Four-lepton production at hadron colliders: aMC@NLO predictions with theoretical uncertainties*, *JHEP* **02** (2012) 099 [arXiv:1110.4738] [INSPIRE].

JHEP10(2022)089